

Confidence Estimation via Auxiliary Models

Charles Corbière, Nicolas Thome, Antoine Saporta, Tuan-Hung Vu, Matthieu Cord, and Patrick Pérez

Abstract—Reliably quantifying the confidence of deep neural classifiers is a challenging yet fundamental requirement for deploying such models in safety-critical applications. In this paper, we introduce a novel target criterion for model confidence, namely the true class probability (TCP). We show that TCP offers better properties for confidence estimation than standard maximum class probability (MCP). Since the true class is by essence unknown at test time, we propose to learn TCP criterion from data with an auxiliary model, introducing a specific learning scheme adapted to this context. We evaluate our approach on the task of failure prediction and of self-training with pseudo-labels for domain adaptation, which both necessitate effective confidence estimates. Extensive experiments are conducted for validating the relevance of the proposed approach in each task. We study various network architectures and experiment with small and large datasets for image classification and semantic segmentation. In every tested benchmark, our approach outperforms strong baselines.

Index Terms—Confidence Estimation, Uncertainty, Deep Neural Networks, Classification with Reject Option, Misclassification Detection, Failure Prediction, Self-Training, Pseudo-Labeling, Unsupervised Domain Adaptation, Semantic Image Segmentation

1 INTRODUCTION

LAST decade's research in deep learning lead to tremendous boosts in predictive performance for various tasks including image classification [1], object recognition [2], [3], [4], natural language processing [5], [6] and speech recognition [7], [8]. However, safety remains a great concern when it comes to implementing these models in real-world conditions [9], [10]. Failing to detect possible errors or overestimating the confidence of a prediction may carry serious repercussions in critical visual-recognition applications such as in autonomous driving, medical diagnosis [11] or nuclear power plant monitoring [12].

Classification with a reject option [13], [14], [15], also known as *selective classification* [16], [17], consists in a scenario where the classifier is given the option to reject an instance instead of predicting its label. Equipped with a reject option, a classifier could decide to stick to the prediction or, on the contrary, to hand over to a human or a back-up system with, *e.g.*, other sensors, or simply to trigger an alarm. One common approach for tackling the problem is to discriminate with a confidence-based criterion: For an instance x , along with a prediction $f(x)$, a scalar value $g(x)$ that quantifies the confidence of the classifier in its prediction is also provided.

Correctly identifying uncertain predictions thanks to low confidence values $g(x)$ could be beneficial for classification improvements in active learning [18] or for efficient exploration in reinforcement learning [19]. On a related matter, one would expect the confidence criterion to correlate successful predictions with high values. Some paradigms, such as self-training with pseudo-labeling [20], [21], consist in picking and labeling the most confident samples before retraining the network accordingly. The performance improves by selecting successful predictions thanks to an accurate confidence criterion. A final perspective, linked to failure prediction [22], [23], [24], is the capacity of models to provide a ranking which enables to distinguish correct from erroneous predictions. In each of the previous tasks, obtaining reliable estimates of the predictive confidence is then of prime importance.

Confidence estimation has been explored in a wide variety of applications, including computer vision [23], [25], speech recognition [26], [27], [28], reinforcement learning [19] or machine translation [29]. A widely used baseline with neural-network classifiers is to take the value of the predicted class' probability, namely the *maximum class probability* (MCP), given by the softmax layer output. Although recent evaluations of MCP with modern deep models reveal reasonable performances [23], they still suffer from several conceptual drawbacks. In particular, MCP leads by design to high confidence values, even for erroneous predictions, since the largest softmax output is used. This design tends to make erroneous and correct predictions overlap in terms of confidence and thus limits the capacity to distinguish them.

In this work, we identify a better confidence criterion, the *true class probability* (TCP), for deep neural network classifiers with a reject option. For a sample x , TCP corresponds to the probability of the model with respect to the true class y of that sample, which naturally reflects a better-behaved model's confidence. We provide theoretical guarantees of the quality of this criterion regarding confidence estimation. Since the true class is obviously unknown at test time, we propose a novel approach which consists in designing an auxiliary network specifically dedicated to estimate the confidence of a prediction. Given a trained classifier f , this auxiliary network learns the TCP criterion from data. In inference, we use its scalar output as the confidence estimate $g(x)$ associated to the prediction. When applied to failure prediction, we observe significant improvements over strong baselines. Our approach is also adequate for self-training strategies in unsupervised domain adaption. To meet the challenge of this task in semantic segmentation, we propose an enhanced architecture with structured output and adopt an adversarial learning scheme which enforces alignment between confidence maps in source and target domains. A thorough analysis of our approach, including relevant variations, ablation studies and qualitative evaluations of confidence estimates, helps to gain insight about its behavior.

In summary, our contributions are as follows:

- We define a novel confidence criterion, the *true class probability*, which exhibits an adequate behavior for confidence estimation;
- We propose to design an auxiliary neural network, coined *ConfidNet*, which aims to learn this confidence criterion from data;
- We apply this approach to the task of failure prediction and to self-training in unsupervised domain adaptation with adequate choices of architecture, loss function and learning scheme;
- We extensively experiment across various benchmarks and backbone networks to validate the relevance of our approach on both tasks.

The paper is organized as follows. In Section 2, we provide an overview of the most relevant related works on confidence estimation, failure prediction, self-training and unsupervised domain adaption. Section 3 exposes our approach for confidence estimation based on learning an adequate criterion via an auxiliary network. We also describe how it relates to classification with a reject option. In Section 4, we adapt our approach to failure prediction by introducing an architecture, a loss function and a learning scheme for this task. Similarly, Section 5 details the instantiation of our approach for confidence-based self-training in unsupervised domain adaptation (DA), which we denote as ConDA. In particular, we present two additions, an adversarial loss and a multi-scale confidence architecture, which help further improving the performance for this task. Finally, we report experimental studies in Section 6. This paper extends a previous conference publication [30] by introducing: (1) An comprehensive adaptation of the approach to improve the key step of self-training from pseudo-labels in semantic segmentation with DA; (2) An exploration of the classification-with-rejection framework, which strengthens the rationale of the proposed approach.

2 RELATED WORK

2.1 Confidence estimation

Confidence estimation in machine learning has been around for many decades, firstly linked to the idea of classification with a reject option [13]. Following works [14], [15], [31], [32] explored alternative rejection criteria. In particular, [31] proposes to jointly learn the classifier and the selection function. El-Yaniv [16] provides an analysis of the risk-coverage trade-off that occurs when classifying with a reject option. More recently, [17], [33] extend the approach to deep neural networks, considering various confidence measures.

Since the wide adoption of deep learning methods, confidence estimation has raised even more interest as recent works reveal that modern neural networks tend to be overconfident [34], non-calibrated [35], [36], sensitive to adversarial attacks [37], [38] and inadequate to distinguish in- from out-of-distribution examples [23], [39], [40].

Bayesian neural networks [41] offer a principled approach for confidence estimation by adopting a Bayesian formalism which models the weight posterior distribution. As the true posterior cannot be evaluated analytically in

complex models, various approximations have been developed, such as variational inference [19], [42], [43] or expectation propagation [44]. In particular, MC Dropout [19] has raised a lot of interest due to the simplicity of its implementation. Predictions are obtained by averaging softmax vectors from multiple feed-forward passes through the network with dropout layers. When applied to regression, the predictive distribution uncertainty can be summarized by computing statistics, *e.g.*, variance. However, when using MC Dropout for uncertainty estimation in classification tasks, the predictive distribution is averaged to a point-wise softmax estimate before computing standard uncertainty criteria, *e.g.* entropy or variants such as mutual information. It is worth mentioning that these entropy-based criteria measure the softmax output dispersion, where the uniform distribution has maximum entropy. It is not clear how well these dispersion measures are adapted to distinguishing failures from correct predictions, especially with deep neural networks which output overconfident predictions [35]: for example, it might be very challenging to discriminate a peaky prediction corresponding to a correct prediction from an incorrect overconfident one. Lakshminarayanan *et al.* [40] propose an alternative to Bayesian neural networks by leveraging an ensemble of neural networks to produce well-calibrated uncertainty estimates. However, it requires to train multiple classifiers, which has a considerable computing cost in training and inference time.

2.2 Failure prediction

In the context of classification, a widely used baseline for failure prediction is to take the value of the predicted class' probability given by the softmax layer output, namely the *maximum class probability* (MCP), suggested by [45] and revised by [23]. As stated before, MCP presents several limits regarding both failure prediction and out-of-distribution detection, as it outputs unduly high confidence values.

Blatz *et al.* [29] introduce a method for confidence estimation in machine translation by solving a binary classification between correct and erroneous predictions. More recently, Jiang *et al.* [24] proposed a new confidence measure, 'Trust Score', which measures the agreement between the classifier and a modified nearest-neighbor classifier on the test examples. More precisely, the confidence criterion used in Trust Score is the ratio between the distance from the sample to the nearest class different from the predicted class and the distance to the predicted class. One clear drawback of this approach is its lack of scalability, since computing nearest neighbors in large datasets is extremely costly in both computations and memory. Another more fundamental limitation related to the Trust Score itself is that local distance computation becomes less meaningful in high dimensional spaces [46], which is likely to negatively affect the performances of this method as shown in Section 6.1.

In tasks closely related to failure prediction, Guo *et al.* [35], for confidence calibration, and Liang *et al.* [39], for out-of-distribution detection, proposed to use temperature scaling to mitigate confidence values. However, this does not affect the ranking of the confidence score and therefore the separability between errors and correct predictions. DeVries *et al.* [47] share with us the same purpose of learning

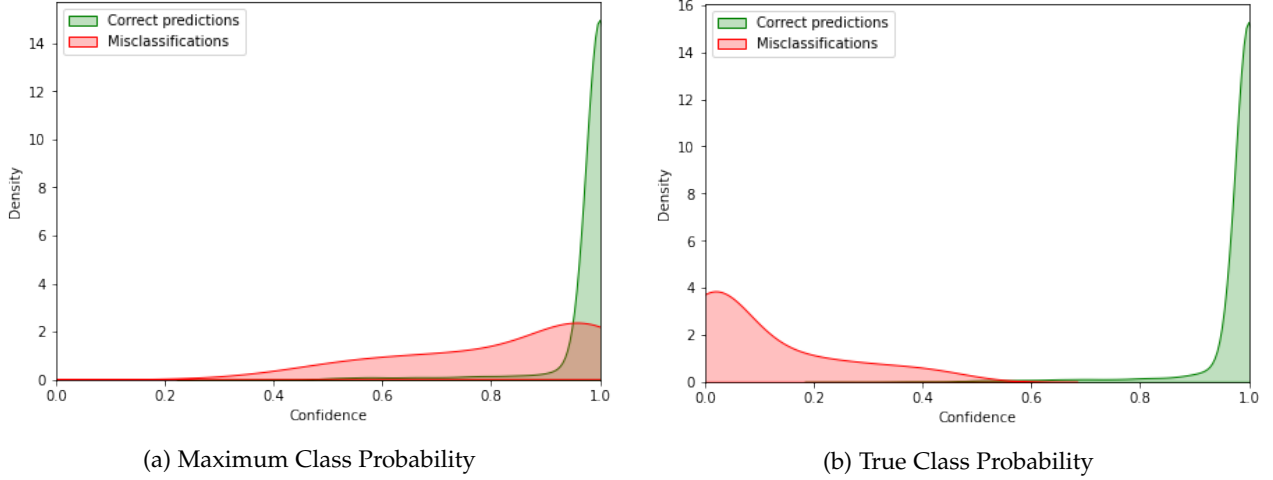


Fig. 1: **Distributions of different confidence measures over correct and erroneous predictions of a given model.** When ranking according to MCP (a) the test predictions of a convolutional model trained on CIFAR-10, we observe that correct ones (in green) and misclassifications (in red) overlap considerably, making it difficult to distinguish them. On the other hand, ranking samples according to TCP (b) alleviates this issue and allows a much better separation.

confidence in neural networks. Their work differs from ours by focusing on out-of-distribution detection and learning jointly a distribution confidence score and classification probabilities. In addition, their criterion is based on an interpolation between output probabilities and target distribution whereas we specifically define a criterion suited to failure prediction.

2.3 Self-training in domain adaptation

Unsupervised Domain Adaptation (UDA). UDA has received a lot of attention over the past few years because of its importance for a variety of real-world problems, such as robotics or autonomous driving. Most works in this line of research aim at minimizing the discrepancy between the data distributions in source and target domains. For the semantic segmentation task, most recent progresses have been obtained by adopting an adversarial training approach to produce indistinguishable source-target distributions in the space of features extracted by modern convolutional deep neural nets. To cite a few methods: CyCADA [48] first stylizes the source-domain images as target-domain images before aligning source and target in the feature space; AdaptSegNet [49] constructs a multi-level adversarial network to perform output-space domain adaptation at different feature levels; AdvEnt [50] aligns the entropy of the pixel-wise predictions with an adversarial loss; BDL [21] learns alternatively an image translation model and a segmentation model that promote each other.

Self-Training. Semi-supervised learning designates the general problem where a decision rule must be learned from both labeled and unlabeled data. Among the methods applied to address this problem, self-training with pseudo-labeling [20] is a simple strategy that relies on picking up the current predictions on the unlabeled data and using them as if they were true labels for further training. It is shown in [20] that the effect of pseudo-labeling is equivalent to entropy regularization [51]. In a UDA setting, the idea is to collect pseudo-labels on the unlabeled target-domain

samples in order to have an additional supervision loss in the target domain. To select only reliable pseudo-labels, such that the performance of the adapted semantic segmentation network effectively improves, BDL [21] resorts to standard selection with MCP. ESL [52] uses instead the entropy of the prediction as confidence criterion for its pseudo-label selection. CBST [53] proposes an iterative self-training procedure where the pseudo-labels are generated based on a loss minimization. In [53], the authors also propose a way to balance the classes in their pseudo-labels to avoid the dominance of large classes as well as a way to introduce spatial priors. More recently, the CRST framework [54] proposes multiple types of confidence regularization to limit the propagation of errors caused by noisy pseudo-labels.

3 LEARNING A MODEL'S CONFIDENCE WITH AN AUXILIARY MODEL

In this section, we first introduce briefly the task of classification with a reject option, along with necessary notations. We then introduce an effective confidence-rate function for neural-net classifiers and we present our approach to learn this target confidence-rate function thanks to an auxiliary neural network. For sake of simplicity, we consider in this section a generic classification task, where the input is raw or transformed signals and the expected output is a predicted category. The semantic segmentation task we address in Section 5 is in effect a pixel-wise classification of localized features derived from the input image.

3.1 Problem formulation

Let us consider a dataset $\mathcal{D} = \{(\mathbf{x}_n, y_n)\}_{n=1}^N$ composed of N *i.i.d.* training samples, where $\mathbf{x}_n \in \mathcal{X} \subset \mathbb{R}^D$ is a D -dimensional data representation, deep feature maps from an image or the image itself for instance, and $y_n \in \mathcal{Y} = \llbracket 1, K \rrbracket$ is its true class among the K pre-defined categories. These samples are drawn from an unknown joint distribution $P(\mathbf{X}, Y)$ over $(\mathcal{X}, \mathcal{Y})$.

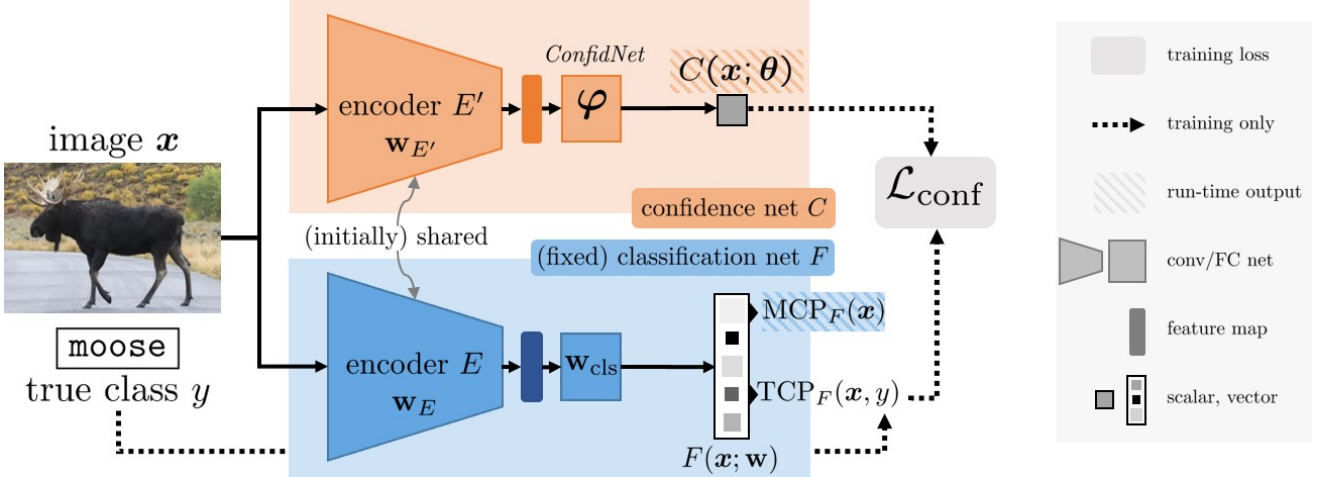


Fig. 2: **Learning confidence approach.** The fixed classification network F , with parameters $\mathbf{w} = (\mathbf{w}_E, \mathbf{w}_{\text{cls}})$, is composed of a succession of convolutional and fully-connected layers (encoder E) followed by last classification layers with softmax activation. The auxiliary confidence network C , with parameters θ , builds upon the feature maps extracted by the encoder E , or its fine-tuned version E' with parameters $\mathbf{w}_{E'}$: they are passed to ConfidNet, a trainable multi-layer module with parameters φ . The auxiliary model outputs a confidence score $C(\mathbf{x}; \theta) \in [0, 1]$, with $\theta = \varphi$ in absence of encoder fine-tuning and $\theta = (\mathbf{w}_{E'}, \varphi)$ in case of fine-tuning.

A *selective classifier* [16], [17] is a pair (f, g) where $f : \mathcal{X} \rightarrow \mathcal{Y}$ is a *prediction function* and $g : \mathcal{X} \rightarrow \{0, 1\}$ is a *selection function* which enables to reject a prediction:

$$(f, g)(\mathbf{x}) = \begin{cases} f(\mathbf{x}), & \text{if } g(\mathbf{x}) = 1, \\ \text{reject}, & \text{if } g(\mathbf{x}) = 0. \end{cases} \quad (1)$$

In this work, we focus on classifiers based on artificial neural networks. Given an input \mathbf{x} , such a network F with parameters \mathbf{w} outputs non-negative scores over all classes, which are L_1 -normalized through softmax. If well trained, this output can be interpreted as the predictive distribution $P(Y|\mathbf{x}, \hat{\mathbf{w}}) = F(\mathbf{x}; \hat{\mathbf{w}}) \in \Delta$, with Δ the probability K -simplex in \mathbb{R}^K and $\hat{\mathbf{w}}$ the learned weights. Based on this distribution, the predicted sample class is usually the maximum *a posteriori* estimate:

$$f(\mathbf{x}) = \operatorname{argmax}_{k \in \mathcal{Y}} P(Y = k|\mathbf{x}, \hat{\mathbf{w}}) = \operatorname{argmax}_{k \in \mathcal{Y}} F(\mathbf{x}; \hat{\mathbf{w}})[k]. \quad (2)$$

We are not interested here in trying to improve the accuracy of the already-trained model F , but rather to make its future use more reliable by endowing the system with the ability to recognize when the prediction might be wrong. To this end, a *confidence-rate function* $\kappa_f : \mathcal{X} \rightarrow \mathbb{R}^+$ is associated to f so as to assess the degree of confidence of its predictions, the higher the value the more certain the prediction [16], [17]. A suitable confidence-rate function should correlate erroneous predictions with low values and successful predictions with high values. Finally, given a user-defined threshold $\delta \in \mathbb{R}^+$, the selection function g can be simply derived from the confidence rate:

$$g(\mathbf{x}) = \begin{cases} 1 & \text{if } \kappa_f(\mathbf{x}) \geq \delta, \\ 0 & \text{otherwise.} \end{cases} \quad (3)$$

3.2 TCP, an effective confidence-rate function

For a given input \mathbf{x} , a standard confidence-rate function for a classifier F is the probability associated to the predicted max-score class, that is the *maximum class probability*:

$$\text{MCP}_F(\mathbf{x}) = \max_{k \in \mathcal{Y}} P(Y = k|\mathbf{x}, \hat{\mathbf{w}}) = \max_{k \in \mathcal{Y}} F(\mathbf{x}; \hat{\mathbf{w}})[k]. \quad (4)$$

However, by taking the largest softmax probability as confidence estimate, MCP leads to high confidence values both for correct and erroneous predictions alike, making it hard to distinguish them, as shown in Figure 1a. On the other hand, when the model misclassifies an example, the probability associated to the true class y is lower than the maximum one and likely to be low. Based on this simple observation, we propose to consider instead this *true class probability* as a suitable confidence-rate function. For any admissible input $\mathbf{x} \in \mathcal{X}$, we assume the *true class* $y(\mathbf{x})$ is known, which we denote y for simplicity. The TCP confident rate is defined as

$$\text{TCP}_F(\mathbf{x}, y) = P(Y = y|\mathbf{x}, \hat{\mathbf{w}}) = F(\mathbf{x}; \hat{\mathbf{w}})[y]. \quad (5)$$

Theoretical guarantees. With TCP, the following properties hold (see derivation in Appendix A.1). Given a properly labelled example (\mathbf{x}, y) , then:

- $\text{TCP}_F(\mathbf{x}, y) > 1/2 \Rightarrow f(\mathbf{x}) = y$, i.e. the example is correctly classified by the model;
- $\text{TCP}_F(\mathbf{x}, y) < 1/K \Rightarrow f(\mathbf{x}) \neq y$, i.e. the example is wrongly classified by the model,

where class prediction $f(\mathbf{x})$ is defined by (2).

Within the range $[1/K, 1/2]$, there is no theoretical guarantee that correct and incorrect predictions will not overlap in terms of TCP. However, when using deep neural networks, we observe that the actual overlap area is extremely small in practice, as illustrated in Figure 1b on the CIFAR-10 dataset. One possible explanation comes from the fact that modern deep neural networks output overconfident

predictions and therefore non-calibrated probabilities [35]. We provide consolidated results and analyses on this aspect in Section 6 and in Appendix A.2.

3.3 Learning to predict TCP with a neural network

Using TCP as confidence-rate function on a model’s output would be of great help when it comes to reliably estimate its confidence. However, the true classes y are obviously not available when estimating confidence on test inputs.

We propose to *learn TCP confidence from data*. More formally, for the classification task at hand, we consider a parametric selective classifier (f, g) , with f based on an already-trained neural network F . We aim at deriving its companion selection function g from a learned estimate of the TCP function of F . To this end, we introduce an *auxiliary model* C , with parameters θ , that is intended to predict TCP_F and to act as confidence-rate function for the selection function g . An overview of the proposed approach is available in Figure 2. This model is trained such that, at runtime, for an input $\mathbf{x} \in \mathcal{X}$ with (unknown) true label y , we have:

$$C(\mathbf{x}; \theta) \approx \text{TCP}_F(\mathbf{x}, y). \quad (6)$$

In practice, this auxiliary model C will be a neural network trained under full supervision on \mathcal{D} to produce this confidence estimate. To design this network, we can transfer knowledge from the already-trained classification network. Throughout its training, F has indeed learned to extract increasingly-complex features that are fed to its final classification layers. Calling E the encoder part of F , a simple way to transfer knowledge consists in defining and training a multi-layer head with parameters φ that regresses TCP_F from features encoded by E . We call *ConfidNet* this module. As a result of this design, the complete confidence network C is composed of a frozen encoder followed by trained ConfidNet layers. As we shall see in Section 4, the complete architecture might be later fine-tuned, including the encoder, as in classic transfer learning. In that case, θ will encompass the parameters of both the encoder and the ConfidNet’s layers.

In the rest of the paper, we detail the different network architectures, loss functions and learning schemes of ConfidNet for two distinct applications: Classification failure prediction and self-training for semantic segmentation with domain adaptation. In both tasks, a ranking of unlabelled samples that allows a clear distinction of correct predictions from erroneous ones is crucial. The proposed auxiliary model offers a new solution to this problem.

4 APPLICATION TO FAILURE PREDICTION

Given a trained model, failure prediction is the task of predicting at run-time whether the model has taken a correct decision or not for a given input. As discussed in Section 2, they are different ways to attack this task, which has many real-world applications in safety-critical systems especially. With a confidence-rate function in hand, the task can be simply set as thresholding this function, exactly in the same way the selection function works in prediction with a reject option. In this Section, we discuss how ConfidNet can be used for that exact purpose in the context of image classification.

4.1 Architecture

State-of-art image classification models are composed of convolutional layers followed by one or more fully-connected layers and a final softmax operation. In order to work with such a classification network F , we build ConfidNet upon a late intermediate representation of F . ConfidNet is designed as a small multilayer perceptron composed of a succession of dense layers with a final sigmoid activation that outputs $C(\mathbf{x}; \theta) \in [0, 1]$. As explained in Section 3, we will train this network in a supervised manner, such that it predicts well the true-class probability assigned by F to the input image. Regarding the capacity of ConfidNet, we have empirically found that increasing further its depth leaves performance unchanged for estimating the confidence of the classification network (see Appendix B.4 for more details).

4.2 Loss function

As we want to regress a score between 0 and 1, we use a mean-square-error (MSE) loss to train the confidence model:

$$\mathcal{L}_{\text{conf}}(\theta; \mathcal{D}) = \frac{1}{N} \sum_{n=1}^N (C(\mathbf{x}_n; \theta) - \text{TCP}_F(\mathbf{x}_n, y_n))^2. \quad (7)$$

Since the final task here is the prediction of failures, with confidence prediction being only a means toward it, a more explicit supervision with failure/success information could be considered. In that case, the previous regression loss could still be used, with 0 (failure) and 1 (success) target values instead of TCP. Alternatively, a binary cross entropy loss (BCE) for the error-prediction task using the predicted confidence as a score could be used. Seeing failure detection as a ranking problem, where good predictions must be ranked before erroneous ones according to the predicted confidence, a batch-wise ranking loss can also be utilized [55]. We assessed experimental all these alternative losses, including a focal version [56] of the BCE to focus on hard examples, as discussed in Section 6.1.3. They lead to inferior performance compared to using (7). This might be due to the fact that TCP conveys more detailed information than a mere binary label on the quality of the classifier’s prediction for a sample. In situations where only very few error samples are available, this fine-grained information improves the performance of the final failure detection (see Section 6.1.3).

4.3 Learning scheme

We decompose the parameters of the classification network F into $\mathbf{w} = (\mathbf{w}_E, \mathbf{w}_{\text{cls}})$, where \mathbf{w}_E denotes its encoder’s weights and \mathbf{w}_{cls} the weights of its last classification layers. Such as in transfer learning, the training of the confidence network C starts by fixing the shared encoder and training only ConfidNet’s weights φ . In this phase, the loss (7) is thus minimized only w.r.t. $\theta = \varphi$.

In a second phase, we further fine-tune the complete network C , including its encoder which is now untied from the classification encoder E (the main classification model must remain unchanged, by definition of the addressed problem). Denoting E' this now independent encoder, and $\mathbf{w}_{E'}$ its weights, this second training phase optimizes (7) w.r.t. $\theta = (\mathbf{w}_{E'}, \varphi)$ with $\mathbf{w}_{E'}$ initially set to \mathbf{w}_E .

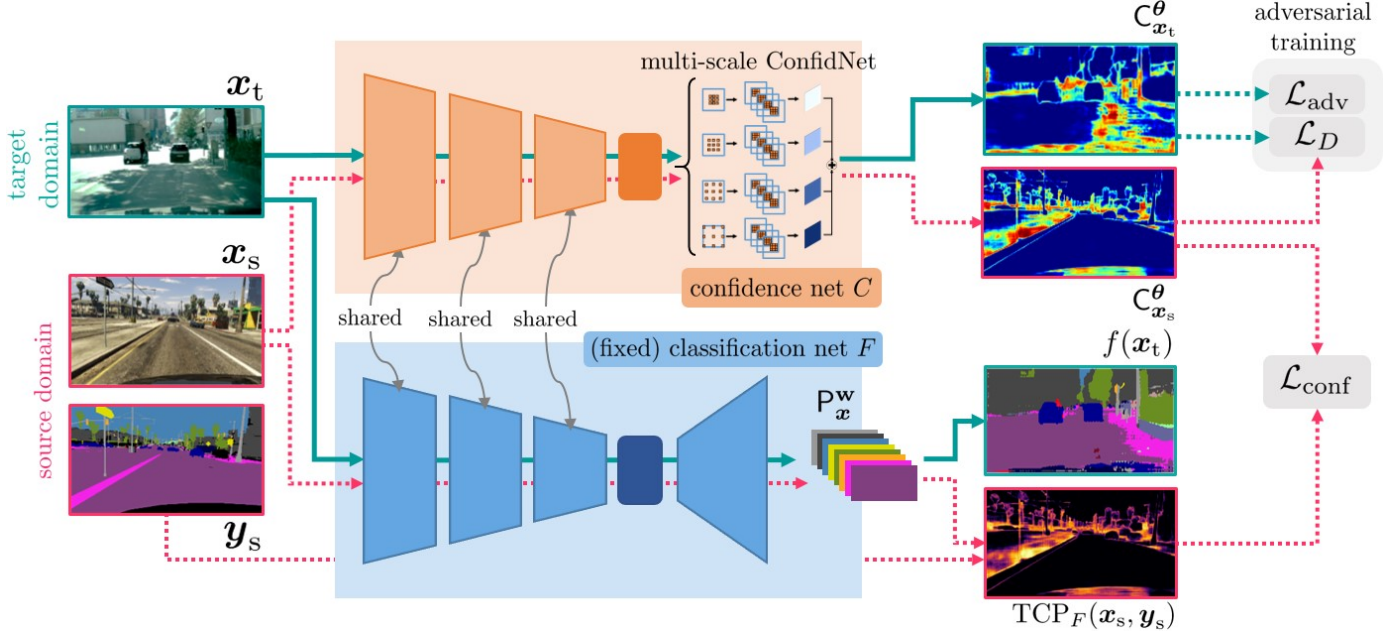


Fig. 3: **Overview of proposed confidence learning for domain adaptation (ConDA) in semantic segmentation.** Given images in source and target domains, we pass them to the encoder part of the segmentation network F to obtain their feature maps. This network F is fixed during this phase and its weights are not updated. The confidence maps are obtained by feeding these feature maps to the trainable head of the confidence network C , which includes a multi-scale ConfidNet module. For source-domain images, a regression loss $\mathcal{L}_{\text{conf}}$ (8) is computed to minimize the distance between $C_{x_s}^\theta$ and the fixed true-class-probability map $\text{TCP}_F(x_s, y_s)$. An adversarial training scheme – based on discriminator's loss $\mathcal{L}_D(\psi)$ (Eq. 10) and adversarial part $\mathcal{L}_{\text{adv}}(\theta)$ of confidence net's loss (Eq. 12) – is also added to enforce the consistency between the $C_{x_s}^\theta$'s and $C_{x_t}^\theta$'s. Dashed arrows stand for paths that are used only at train time.

We also deactivate dropout layers in this last training phase and reduce learning rate to mitigate stochastic effects that may lead the new encoder to deviate too much from the original one used for classification. Data augmentation can thus still be used.

In Section 6, we put this framework at work on several standard image-classification benchmarks and analyse its effectiveness in comparison with alternative approaches.

5 APPLICATION TO SELF-TRAINING IN SEMANTIC SEGMENTATION WITH DOMAIN ADAPTATION

Unsupervised domain adaptation for semantic segmentation aims to adapt a segmentation model trained on a labeled source domain to a target domain devoid of annotation. Formally, let us consider the annotated source-domain training set $\mathcal{D}_s = \{(\mathbf{x}_{s,n}, \mathbf{y}_{s,n})\}_{n=1}^{N_s}$, where $\mathbf{x}_{s,n}$ is a color image of size (H, W) and $\mathbf{y}_{s,n} \in \mathcal{Y}^{H \times W}$ its associated ground-truth segmentation map. A segmentation network F with parameters \mathbf{w} takes as input an image \mathbf{x} and returns a predicted soft-segmentation map $F(\mathbf{x}; \mathbf{w}) = \mathbf{P}_{\mathbf{x}}^{\mathbf{w}} \in [0, 1]^{H \times W \times K}$, where $\mathbf{P}_{\mathbf{x}}^{\mathbf{w}}[h, w, :] = P(Y[h, w] | \mathbf{x}; \mathbf{w}) \in \Delta$. The final prediction of the network is the segmentation map $f(\mathbf{x})$ defined pixel-wise as $f(\mathbf{x})[h, w] = \text{argmax}_{k \in \mathcal{Y}} \mathbf{P}_{\mathbf{x}}^{\mathbf{w}}[h, w, k]$. This network is learned with full supervision from the source-domain samples in \mathcal{D}_s , using a cross-entropy loss, while leveraging a set \mathcal{D}_t of unlabeled target-domain examples.

5.1 Self-training for unsupervised domain adaptation

In UDA, the main challenge is to use the unlabeled target set $\mathcal{D}_t = \{\mathbf{x}_{t,n}\}_{n=1}^{N_t}$ available during training to learn domain-invariant features on which the segmentation model would behave similarly in both domains. As reviewed in Section 2, a variety of techniques have been proposed to do that, in particular for the task of semantic segmentation. Leveraging automatic pseudo-labeling of target-domain training examples is in particular a simple, yet powerful way to further improve UDA performance with self-training. One key ingredient of such an approach being the selection of the most promising pseudo-labels, the proposed auxiliary confidence-prediction model lends itself particularly well to this task. In the rest of this section, we detail how the proposed approach to confidence prediction can be adapted to semantic segmentation, with application to domain adaptation through self-training. The resulting framework, called ConDA, is illustrated in Figure 3.

A high-level view of self-training for semantic segmentation with UDA is as follows:

- 1) Train a segmentation network for the target domain using a chosen UDA technique;
- 2) Collect pseudo-labels among the predictions that this network makes on the target-domain training images;
- 3) Train a new semantic-segmentation network from scratch using the chosen UDA technique in combination with supervised training on target-domain

data with pseudo-labels;

4) Possibly, repeat from step 2 by collecting better pseudo-labels after each iteration.

While the general idea of self-training is simple and intuitive, collecting good pseudo-labels is quite tricky: If too many of them correspond to erroneous predictions of the current segmentation network, the performance of the whole UDA can deteriorate. Thus, a measure of confidence should be used in order to only gather reliable predictions as pseudo-labels and to reject the others.

5.2 Selecting pseudo-labels with a confidence model

Following the self-training framework previously described, a confidence network C is learned at step (2) to predict the confidence of the UDA-trained semantic segmentation network F and used to select only trustworthy pseudo-labels on target-domain images. To this end, the framework proposed in Section 3 in an image classification setup, and applied to predicting erroneous image classification in Section 4, needs here to be adapted to the structured output of semantic segmentation.

Semantic segmentation can be seen as a pixel-wise classification problem. Given a target-domain image \mathbf{x}_t , we want to predict both its soft semantic map $F(\mathbf{x}_t; \mathbf{w})$ and, using an auxiliary model with trainable parameters θ , its confidence map $C(\mathbf{x}_t; \theta) = C_{\mathbf{x}_t}^\theta \in [0, 1]^{H \times W}$. Given a pixel (h, w) , if its confidence $C_{\mathbf{x}_t}^\theta[h, w]$ is above a chosen threshold δ , we label it with its predicted class $f(\mathbf{x}_t)[h, w] = \text{argmax}_{k \in \mathcal{Y}} P_{\mathbf{x}_t}^{\mathbf{w}}[h, w, k]$, otherwise it is masked out. Computed over all images in \mathcal{D}_t , these incomplete segmentation maps, constitute target pseudo-labels that are used to train a new semantic-segmentation network. Optionally, we may repeat from step (2) and learn alternately a confidence model to collect pseudo-labels and a segmentation network using this self-training.

5.3 Confidence training with adversarial loss

To train the segmentation confidence network C , we propose to jointly optimize two objectives. Following the approach proposed in Section 3, the first one supervises the confidence prediction on annotated source-domain examples using the known true class probabilities for the predictions from F . Specific to semantic segmentation with UDA, the second one is an adversarial loss that aims at reducing the domain gap between source and target. A complete overview of the approach is provided in Figure 3.

Confidence loss. The first objective is a pixel-wise version of the confidence loss in (7). On annotated source-domain images, it requires C to predict at each pixel the score assigned by F to the (known) true class:

$$\mathcal{L}_{\text{conf}}(\theta; \mathcal{D}_s) = \frac{1}{N_s} \sum_{n=1}^{N_s} \|C_{\mathbf{x}_{s,n}}^\theta - \text{TCP}_F(\mathbf{x}_{s,n}, \mathbf{y}_{s,n})\|_F^2, \quad (8)$$

where $\|\cdot\|_F$ denotes the Frobenius norm and, for an image \mathbf{x} with true segmentation map \mathbf{y} and predicted soft one $F(\mathbf{x}; \hat{\mathbf{w}})$, we note

$$\text{TCP}_F(\mathbf{x}, \mathbf{y})[h, w] = F(\mathbf{x}; \hat{\mathbf{w}})[h, w, \mathbf{y}[h, w]] \quad (9)$$

at location (h, w) . On a new input image, C should predict at each pixel the score that F will assign to the unknown true class, which will serve as a confidence measure.

However, compared to the application in previous Section, we have here the additional problem of the gap between source and target domains, an issue that might affect the training of the confidence model as in the training of the segmentation model.

Adversarial loss. The second objective concerns the domain gap. While model C learns to estimate TCP on source-domain images, its confidence estimation on target-domain images may suffer dramatically from this domain shift. As classically done in UDA, we propose an adversarial learning of our auxiliary model in order to address this problem. More precisely, we want the confidence maps produced by C in the source domain to resemble those obtained in the target domain.

A discriminator $D : [0, 1]^{H \times W} \rightarrow \{0, 1\}$, with parameters ψ , is trained concurrently with C with the aim to recognize the domain (1 for source, 0 for target) of an image given its confidence map. The following loss is minimized w.r.t. ψ :

$$\mathcal{L}_D(\psi; \mathcal{D}_s \cup \mathcal{D}_t) = \frac{1}{N_s} \sum_{n=1}^{N_s} \mathcal{L}_{\text{adv}}(\mathbf{x}_{s,n}, 1) + \frac{1}{N_t} \sum_{n=1}^{N_t} \mathcal{L}_{\text{adv}}(\mathbf{x}_{t,n}, 0), \quad (10)$$

where \mathcal{L}_{adv} denotes the cross-entropy loss of the discriminator based on confidence maps:

$$\mathcal{L}_{\text{adv}}(\mathbf{x}, \lambda) = -\lambda \log(D(C_{\mathbf{x}}^\theta; \psi)) - (1 - \lambda) \log(1 - D(C_{\mathbf{x}}^\theta; \psi)), \quad (11)$$

for $\lambda = \{0, 1\}$, which is a function of both ψ and θ . In alternation with the training of the discriminator using (10), the adversarial training of the confidence net is conducted by minimizing, w.r.t. θ , the following loss:

$$\mathcal{L}_C(\theta; \mathcal{D}_s \cup \mathcal{D}_t) = \mathcal{L}_{\text{conf}}(\theta; \mathcal{D}_s) + \frac{\lambda_{\text{adv}}}{N_t} \sum_{n=1}^{N_t} \mathcal{L}_{\text{adv}}(\mathbf{x}_{t,n}, 1), \quad (12)$$

where the second term, weighted by λ_{adv} , encourages C to produce maps in target domain that will confuse the discriminator.

This adversarial scheme for confidence learning also acts as a regularizer during training, improving the robustness of the unknown TCP target confidence. As the training of C may actually be unstable, adversarial training provides additional information signal, in particular imposing that confidence estimation should be invariant to domain shifts. We empirically observed that this adversarial confidence learning provides better confidence estimates and improves convergence and stability of the training scheme.

5.4 Multi-scale ConfidNet architecture

In semantic segmentation, models consist of fully convolutional networks where hidden representations are 2D feature maps. This is in contrast with the architecture of classification models considered in Section 4. As a result,

TABLE 1: **Comparison of confidence estimation methods for failure prediction and selective classification.** For each dataset, all methods share the same classification network. For MC Dropout, test accuracy is averaged through random sampling. The first three metrics are percentages and concern failure prediction. The two last ones (the lower, the better) concern selective classification and their values have been multiplied by 10^3 for clarity. Best results are in bold, second best ones are underlined.

Dataset	Model	FPR@95% TPR \downarrow	AUPR \uparrow	AUROC \uparrow	AURC \downarrow	E-AURC \downarrow
MNIST MLP	MCP [23]	14.87	37.70	97.13	0.77	0.58
	MC Dropout [19]	15.15	38.22	97.15	0.79	0.59
	Trust Score [24]	<u>12.31</u>	<u>52.18</u>	<u>97.52</u>	<u>0.69</u>	<u>0.50</u>
	ConfidNet	<u>11.79</u>	<u>57.37</u>	<u>97.83</u>	<u>0.63</u>	<u>0.44</u>
MNIST SmallConvNet	MCP [23]	5.56	35.05	98.63	0.17	0.12
	MC Dropout [19]	<u>5.26</u>	<u>38.50</u>	<u>98.65</u>	<u>0.17</u>	<u>0.13</u>
	Trust Score [24]	10.00	35.88	98.20	0.21	0.17
	ConfidNet	<u>3.33</u>	<u>45.89</u>	<u>98.82</u>	<u>0.15</u>	<u>0.11</u>
SVHN SmallConvNet	MCP [23]	<u>31.28</u>	<u>48.18</u>	<u>93.20</u>	<u>5.44</u>	<u>4.38</u>
	MC Dropout [19]	36.60	43.87	92.85	5.68	4.57
	Trust Score [24]	34.74	43.32	92.16	6.08	5.03
	ConfidNet	<u>28.58</u>	<u>50.72</u>	<u>93.44</u>	<u>5.37</u>	<u>4.32</u>
CIFAR-10 VGG16	MCP [23]	<u>47.50</u>	45.36	91.53	10.45	7.32
	MC Dropout [19]	49.02	<u>46.40</u>	<u>92.08</u>	<u>9.97</u>	<u>6.92</u>
	Trust Score [24]	55.70	38.10	88.47	16.04	12.91
	ConfidNet	<u>44.94</u>	<u>49.94</u>	<u>92.12</u>	<u>9.96</u>	<u>6.83</u>
CIFAR-100 VGG16	MCP [23]	67.86	71.99	85.67	120.28	54.35
	MC Dropout [19]	64.68	<u>72.59</u>	<u>86.09</u>	113.16	50.99
	Trust Score [24]	71.74	66.82	84.17	126.90	60.97
	ConfidNet	<u>62.96</u>	<u>73.68</u>	<u>86.28</u>	<u>118.81</u>	<u>52.88</u>

ConfidNet module must have a different design here: Instead of fully-connected layers, it is composed of 1×1 convolutional layers with the adequate number of channels.

In many segmentation datasets, the existence of objects at multiple scales may complicate confidence estimation. As in recent works dealing with varying object sizes [57], we further improve our confidence network C by adding a multi-scale architecture based on spatial pyramid pooling. It consists of a computationally efficient scheme to re-sample a feature map at different scales, and then to aggregate the confidence maps.

From a feature map, we apply parallel atrous convolutional layers with 3×3 kernel size and different sampling rates, each of them followed by a series of 4 standard convolutional layers with 3×3 kernel size. In contrast with convolutional layers with large kernels, atrous convolutional layers enlarge the field of view of filters and help to incorporate a larger context without increasing the number of parameters and the computation time. Resulting features are then summed before upsampling to the original image size of $H \times W$. We apply a final sigmoid activation to output a confidence map with values between 0 and 1.

The whole architecture of the confidence model C is represented in the orange block of Figure 3, along with its training given a fixed segmentation model F (blue block) with which it shares the encoder. Such as in previous section, fine-tuning the encoder within C is also possible, although we did not explore the option in this semantic segmentation context due to the excessive memory overhead it implies.

6 EXPERIMENTS

We evaluate our approach on the two tasks presented in previous sections: Failure prediction in classification settings and semantic segmentation with domain adaptation.

6.1 Failure prediction

In this section, we present comparative experiments against state-of-the-art confidence-estimation approaches and Bayesian methods on various datasets. Then, we study the effect of learning variants on our approach.

6.1.1 Experimental setup

The experiments are conducted on image datasets of varying scale and complexity: MNIST [58] and SVHN [59] datasets provide small and relatively simple images of digits (10 classes). CIFAR-10 and CIFAR-100 [60] propose more complex object-recognition tasks on low resolution images.

The classification models range from small convolutional networks for MNIST and SVHN to the larger VGG-16 architecture for the CIFAR datasets. We also consider a multi-layer perceptron (MLP) with one hidden layer to investigate performances on small models. ConfidNet is attached to the penultimate layer of the convolutional neural network. Further details about datasets, architectures, training and metrics can be found in Appendix B.

We measure the quality of failure prediction following standard metrics used in the literature [23]: AUROC, the area under the receiver operating characteristic; FPR@95% TPR, the false-positive rate measured when the true-positive rate is 95%; and AUPR, the area under the precision-recall curve, using here incorrect model's predictions as positive detection samples (see details in Appendix B.2). Among these metrics, AUPR is the most directly related to the failure detection task, and is thus the prevalent one in our assessment.

As an additional, indirect way to assess the quality of the predicted classifier's confidence, we also consider the selective classification problem that was discussed in Section 3.1. In this setup, the predictions by the classifier F that

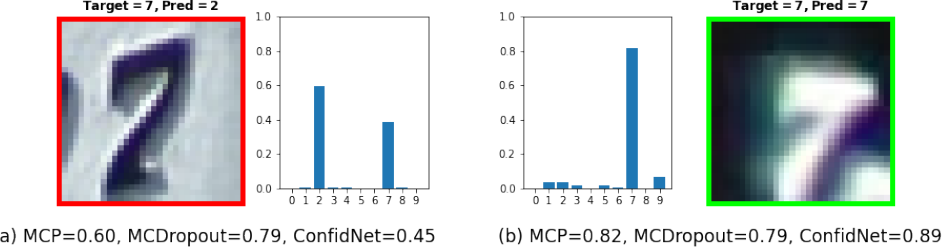


Fig. 4: Limitations of MC Dropout's confidence measure. Two test samples from SVHN dataset, which are respectively misclassified (left) and correctly classified (right) by a given model F , illustrate these limits. The entropies of the predicted class distributions (averaged over Monte Carlo dropout layers and displayed as histograms) are equally high, at around 0.79, resulting in equally low MC Dropout confidence estimates. In contrast, both MCP and TCP approximated by ConfidNet clearly differ as expected for the two examples. Yet, ConfidNet has the best behavior, being the lowest for the erroneous model's prediction and the highest for the correct one.

TABLE 2: Impact of the choice of training data on the error-prediction performance of ConfidNet. Comparison in AUPR between training on model's train set or on a validation set.

Variant	MNIST MLP	MNIST SmallConvNet	SVHN SmallConvNet	CIFAR-10 VGG-16	CIFAR-100 VGG-16
ConfidNet-train	57.34%	43.94%	50.72%	49.94%	73.68%
ConfidNet-val	33.41%	34.22%	47.96%	48.93%	73.85%

get a predicted confidence below a defined threshold are rejected. Given a coverage rate (the fraction of examples that are not rejected), the performance of the classifier should improve. The impact of this selection, and hence of the underlying confidence-rate function, is measured in average with the area under the risk-coverage curve (AURC) and its normalized variant *Excess*-AURC (E-AURC) [61].

6.1.2 Comparative results

Along with our approach, we implemented competitive confidence and uncertainty estimation methods including MCP [23], Trust Score [24], and Monte-Carlo Dropout (MC Dropout) [19].

Comparative results are summarized in Table 1. We observe that our approach outperforms the other methods in every setting, with a significant gap on small datasets. This confirms that TCP is an adequate confidence criterion for failure prediction and that our approach ConfidNet is able to learn it. Trust Score also delivers good results on small datasets/models such as MNIST. While ConfidNet still performs well on more complex datasets, Trust Score's performance drops, which might be explained by high-dimensionality issues with distances. Regarding selective classification result (AURC and E-AURC), we also provide risk-coverage curves in Appendix B.8.

We also improve state-of-art performances from MC Dropout. While MC Dropout leverages ensembling based on dropout layers, taking as confidence measure the entropy on the average softmax distribution may not be always adequate. In Figure 4, we show side-by-side samples with similar distribution entropy. The left image is misclassified while the right one enjoys a correct prediction. In fact, the entropy is a permutation-invariant measure on discrete probability distributions: A correct 3-class prediction with score vector $[0.65, 0.34, 0.01]$ has the same entropy-based confidence as an incorrect one with probabilities $[0.34, 0.65, 0.01]$. In

contrast, our approach can discriminate an incorrect from a correct prediction, despite both having similarly-spread distributions.

6.1.3 Effect of learning variants

We analyse in Table 3 the effect of the encoder fine-tuning that is described in Section 4.3. Learning only ConfidNet on top of the pre-trained encoder E (that is, $\theta = \varphi$), our confidence network already achieves significant improvements w.r.t. the baselines. With a subsequent fine-tuning of both modules (that is $\theta = (\mathbf{w}_E', \varphi)$), its performance is further boosted in every setting, by around 1-2%. Note that using a vanilla fine-tuning without the deactivation of the dropout layers did not bring any improvement.

TABLE 3: Impact of the encoder fine-tuning on the error-prediction performance of ConfidNet. Comparison in AUPR on two benchmarks with different backbones.

	MNIST SmallConvNet	CIFAR-100 VGG-16
Confidence training	43.94%	72.68%
+ Encoder fine-tuning	45.89%	73.68%

Given the small number of erroneous-prediction samples that are available due to deep neural network over-fitting, we also experimented confidence training on a hold-out dataset. We report the results on all datasets in Table 2 for validation sets with 10% of samples. We observe a general performance drop when using a validation set for training TCP confidence. The drop is especially pronounced for small datasets (MNIST), where models reach more than 97% of train and validation accuracies. Consequently, with a high accuracy and a small validation set, we do not get a larger absolute number of errors using a hold-out set rather than the train set. One solution would be to increase

TABLE 4: Comparative performance on semantic segmentation with synth-to-real unsupervised domain adaptation. Results in per-class IoU and class-averaged mIoU on GTA5 \triangleright Cityscapes. All methods are based on a DeepLabv2 backbone.

Method	Self-Train.	GTA5 \triangleright Cityscapes																				mIoU
		road	sidewalk	building	wall	fence	pole	light	sign	veg	terrain	sky	person	rider	car	truck	bus	train	mbike	bike		
AdaptSegNet [49]		86.5	25.9	79.8	22.1	20.0	23.6	33.1	21.8	81.8	25.9	75.9	57.3	26.2	76.3	29.8	32.1	7.2	29.5	32.5	41.4	
CyCADA [48]		86.7	35.6	80.1	19.8	17.5	38.0	39.9	41.5	82.7	27.9	73.6	64.9	19.0	65.0	12.0	28.6	4.5	31.1	42.0	42.7	
DISE [62]		91.5	47.5	82.5	31.3	25.6	33.0	33.7	25.8	82.7	28.8	82.7	62.4	30.8	85.2	27.7	34.5	6.4	25.2	24.4	45.4	
AdvEnt [50]		89.4	33.1	81.0	26.6	26.8	27.2	33.5	24.7	83.9	36.7	78.8	58.7	30.5	84.8	38.5	44.5	1.7	31.6	32.4	45.5	
CBST [53]	✓	91.8	53.5	80.5	32.7	21.0	34.0	28.9	20.4	83.9	34.2	80.9	53.1	24.0	82.7	30.3	35.9	16.0	25.9	42.8	45.9	
MRKLD [54]	✓	91.0	55.4	80.0	33.7	21.4	37.3	32.9	24.5	85.0	34.1	80.8	57.7	24.6	84.1	27.8	30.1	26.9	26.0	42.3	47.1	
BDL [21]	✓	91.0	44.7	84.2	34.6	27.5	30.2	36.0	36.0	85.0	43.6	83.0	58.6	31.6	83.3	35.3	49.7	3.3	28.8	35.6	48.5	
ESL [52]	✓	90.2	43.9	84.7	35.9	28.5	31.2	37.9	34.0	84.5	42.2	83.9	59.0	32.2	81.8	36.7	49.4	1.8	30.6	34.1	48.6	
ConDA	✓	93.5	56.9	85.3	38.6	26.1	34.3	36.9	29.9	85.3	40.6	88.3	58.1	30.3	85.8	39.8	51.0	0.0	28.9	37.8	49.9	

the validation-set size, but this would damage the model’s prediction performance. By contrast, we take care with our experiments to base our confidence estimation on models with levels of test predictive performance that are similar to those of the baselines. On CIFAR-100, the gap between train accuracy and validation accuracy is substantial (95.56% vs. 65.96%), which may explain the slight improvement for confidence estimation using a validation set (+0.17%). We think that training ConfiNet on a validation set with models reporting low/medium test accuracies could improve the approach.

TABLE 5: Effect of the loss on the error-detection performance of ConfiNet. Comparison in AUPR between proposed MSE loss and three other alternatives.

Dataset	MSE	BCE	Focal	Ranking
SVHN	50.72%	50.00%	49.96%	48.11%
CIFAR-10	49.94%	47.95%	47.76%	44.04%

In Table 5, we compare training ConfiNet with the MSE loss (7) to training with a binary-classification cross-entropy loss (BCE), a focal BCE loss and a batch-wise approximate ranking loss. Even though BCE specifically addresses the failure prediction task, it achieves lower performances on CIFAR-10 and SVHN datasets. Similarly, the focal loss and the ranking one yield results below TCP’s performance in every tested benchmark. Our intuition is that TCP regularizes the training by providing finer-grain information about the quality of the classifier’s predictions. This is especially important in the difficult learning configuration where only very few error samples are available due to the good performance of the classifier.

6.2 Unsupervised domain adaptation in semantic segmentation

In this section, we analyse on several semantic segmentation benchmarks the performance of ConDA, our approach to domain adaptation with confidence-based self-training. We report comparisons with state-of-the-art methods on each benchmark. We also analyse further the quality of ConDA’s pseudo-labelling and demonstrate via an ablation study the importance of each of its components.

6.2.1 Experimental setup

As in many UDA works for semantic segmentation, we consider the specific task of adapting from synthetic to real data in urban scenes. We present in particular experiments in the common set-up, denoted GTA5 \triangleright Cityscapes, where GTA5 [63] is the synthetic source dataset while the real-word target dataset is Cityscapes [64]. We also validate our approach on two other benchmarks – SYNTHIA \triangleright Cityscapes and SYNTHIA \triangleright Mapillary Vistas [65] – in Appendix C.3. The GTA5 [63] dataset is composed of 24,966 images extracted from the eponymous game, of dimension 1914×1052 and semantically annotated with 19 classes in common with Cityscapes [64]. Cityscapes [64] is a dataset of real street-level images. For domain adaptation, we use the training set as target dataset during training. It is composed of 2,975 images of dimension 2048×1024 . All results are reported in terms of intersection over union (IoU) per class or mean IoU over all classes (mIoU); the higher this percentage, the better.

We evaluate the proposed self-training method on AdvEnt [50], a state-of-the-art UDA approach. AdvEnt [50] proposes an adversarial learning framework for domain adaptation: Instead of the softmax output predictions, AdvEnt aligns the entropy of the pixel-wise predictions. All the implementations are done with the PyTorch framework [66]. The semantic segmentation models are initialized with DeepLabv2 backbones pretrained on ImageNet [1]. Due to computational constraints, we only train the multi-scale ConfiNet without encoder fine-tuning. Further information about architectures and implementation details of training and metrics can be found in Appendix C.1.

6.2.2 Comparison with state of the art

The results of semantic segmentation on the Cityscapes validation set using GTA5 as source domain are available in Table 4. All the methods rely on DeepLabv2 as their segmentation backbone. We first notice that self-training-based methods from the literature are superior on this benchmark, with performance reaching up to 48.6% mIoU with ESL [52]. ConDA outperforms all those methods by reaching 49.9% mIoU.

6.2.3 Analysis

Ablation Study. To study the effect of the adversarial training and of the multi-scale confidence architecture on

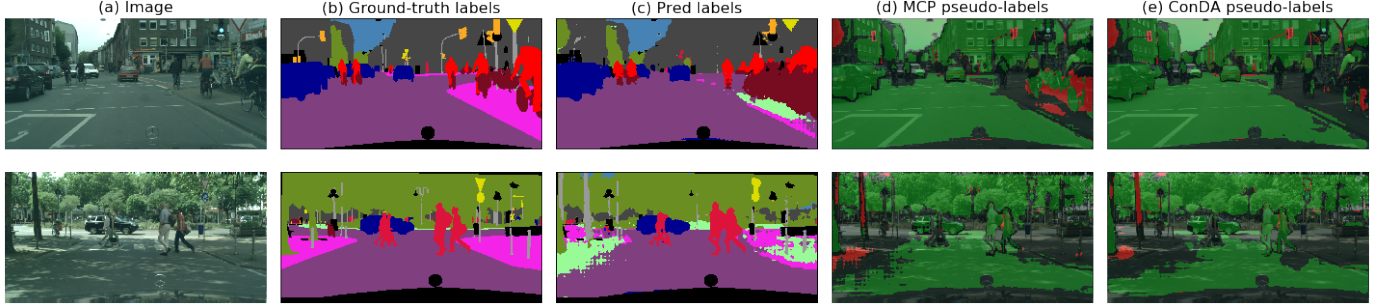


Fig. 5: **Qualitative results of pseudo-label selection for semantic-segmentation adaptation.** The three first columns present target-domain images of the GTA5 \triangleright Cityscapes benchmark (a) along with their ground-truth segmentation maps (b) and the predicted maps before self-training (c). We compare pseudo-labels collected with MCP (d) and with ConDA (e). Green (resp. red) pixels are correct (resp. erroneous) predictions selected by the method and black pixels are discarded predictions. ConDA retains fewer errors while preserving approximately the same amount of correct predictions.

the confidence model, we perform an ablation study on the GTA5 \triangleright Cityscapes benchmark. The results on domain adaptation after re-training the segmentation network using collected pseudo-labels are reported in Table 6. In this table, “ConfidNet” refers to the simple network architecture defined in Section 4 (adapted to segmentation by replacing the fully connected layers by 1×1 convolutions of suitable width); “Adv. ConfidNet” denotes the same architecture but with the adversarial loss from Section 5.3 added to its learning scheme; “Multi-scale ConfidNet” stands for the architecture introduced in Section 5.4; Finally, the full method, “ConDA” amounts to having both this architecture and the adversarial loss. We notice that adding the adversarial learning achieves significantly better performance, for both ConfidNet and multi-scale ConfidNet, with respectively +1.4 and +0.8 point increase. Multi-scale ConfidNet (resp. adv. multi-Scale ConfidNet) also improves performance up to +0.9 point (resp. +0.3) from their ConfidNet architecture counterpart. These results stress the importance of both components of the proposed confidence model.

Model	Multi-Scale.	Adv	mIoU
ConfidNet			47.6
Multi-Scale ConfidNet	✓		48.5
Adv. ConfidNet		✓	49.0
ConDA (Adv. Multi-scale ConfidNet)	✓	✓	49.3

TABLE 6: **Ablation study on semantic segmentation with pseudo-labelling-based adaptation.** Full-fledged ConDA approach is compared on GTA5 \triangleright Cityscapes to stripped-down variants (w/ and w/o multi-scale architecture in ConfidNet, w/ and w/o adversarial learning).

Quality of pseudo-labels. We analyze here the effectiveness of MCP and ConDA as confidence measure to select relevant pseudo-labels in the target domain. For a given fraction of retained pseudo-labels (coverage) on target-domain training images, we compare in Figure 6 the proportion of those labels that are correct (accuracy). ConDA outperforms MCP for all coverage levels, meaning the it selects significantly fewer erroneous predictions for the next round of segmentation-model training. Along with the segmentation adaptation improvements presented earlier, these coverage results demonstrate that reducing the amount of noise in

the pseudo-labels is key to learn a better segmentation adaptation model. Figure 5 presents qualitative results of those pseudo-labels methods. We find again that MCP and ConDA seem to select around the same amount of correct predictions in their pseudo-labels, but with ConDA picking out a lot fewer erroneous ones.

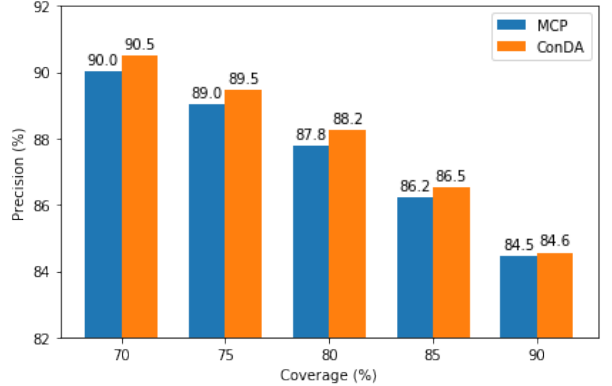


Fig. 6: **Comparative quality of selected pseudo-labels.** Proportion of correct pseudo-labels (precision) for different coverages on GTA5 \triangleright Cityscapes, for MCP and ConDA.

7 CONCLUSION

In this paper, we defined a new confidence criterion, TCP, which enjoys both theoretical guarantees and empirical evidences of improving the confidence estimation for classifiers with a reject option. We proposed a specific method to learn this criterion with an auxiliary neural network built upon the encoder of the model that is monitored. Applied to failure prediction, this learning scheme consists in training the auxiliary network and then enabling the fine-tuning of its encoder (the one of the monitored classifier remains frozen). In each image classification experiment, we were able to improve the capacity of the model to distinguish correct from erroneous samples and to achieve better selective classification. Besides failure prediction, other applications can benefit from this improved confidence estimation. In particular, we showed that applied to self-training with pseudo-labels, our approach reaches state-of-the-art results on three synthetic-to-real unsupervised-domain-adaptation

benchmarks (GTA5 \triangleright Cityscapes, SYNTHIA \triangleright Cityscapes and SYNTHIA \triangleright Mapillary Vistas). To achieve these results, we equipped the auxiliary model with a multi-scale confidence architecture and supplemented the confident loss with an adversarial training scheme which enforces alignment between confidence maps in source and target domains. One clear limitation of this approach is the number of errors available in training. Further work includes exploring methods to artificially generate errors, such as aggressive data augmentation.

APPENDIX A

THE TRUE CLASS PROBABILITY (TCP) CRITERION

A.1 Proof of TCP's theoretical guarantees

Let F be a trained neural network classifier with learned weights $\hat{\mathbf{w}}$ as defined in the main paper, K be the number of labels and $\mathbf{x} \in \mathbb{R}^D$ a sample with its associated true label $y \in \mathcal{Y}$ such that $\text{TCP}_F(\mathbf{x}, y) > \frac{1}{2}$. Starting from the definition of TCP we have:

$$\text{TCP}_F(\mathbf{x}, y) = P(Y = y|\mathbf{x}, \hat{\mathbf{w}}) > \frac{1}{2} \quad (13)$$

$$\iff 1 - \sum_{k \in \mathcal{Y}, k \neq y} P(Y = k|\mathbf{x}, \hat{\mathbf{w}}) > \frac{1}{2} \quad (14)$$

$$\iff \sum_{k \in \mathcal{Y}, k \neq y} P(Y = k|\mathbf{x}, \hat{\mathbf{w}}) < \frac{1}{2}. \quad (15)$$

Since probabilities are positive, we obtain that $\forall k \neq y$, $P(Y = k|\mathbf{x}, \hat{\mathbf{w}}) < \frac{1}{2} < P(Y = y|\mathbf{x}, \hat{\mathbf{w}})$. Denoting \hat{y} the class predicted by the network, we have $\hat{y} = \text{argmax}_k P(Y = k|\mathbf{x}, \hat{\mathbf{w}})$. Hence $\hat{y} = y$.

In the same way, for any $(\mathbf{x}, y) \in \mathbb{R}^D \times \mathcal{Y}$, such that $\text{TCP}_F(\mathbf{x}, y) < \frac{1}{K}$, we have:

$$P(Y = y|\mathbf{x}, \hat{\mathbf{w}}) < \frac{1}{K} \quad (16)$$

$$\iff 1 - \sum_{k \in \mathcal{Y}, k \neq y} P(Y = k|\mathbf{x}, \hat{\mathbf{w}}) < \frac{1}{K} \quad (17)$$

$$\iff \sum_{k \in \mathcal{Y}, k \neq y} P(Y = k|\mathbf{x}, \hat{\mathbf{w}}) > \frac{K-1}{K}. \quad (18)$$

If the model correctly classifies this sample, *i.e.*, $\hat{y} = y$, then $\forall k \neq y$, $P(Y = y|\mathbf{x}, \hat{\mathbf{w}}) \geq P(Y = k|\mathbf{x}, \hat{\mathbf{w}})$. We have:

$$\sum_{k \in \mathcal{Y}, k \neq y} P(Y = k|\mathbf{x}, \hat{\mathbf{w}}) \leq (K-1)P(Y = y|\mathbf{x}, \hat{\mathbf{w}}) \leq \frac{K-1}{K}, \quad (19)$$

which contradicts Equation 18. Hence, there exists at least one k such that $P(Y = k|\mathbf{x}, \hat{\mathbf{w}}) > P(Y = y|\mathbf{x}, \hat{\mathbf{w}})$, which results in $\hat{y} \neq y$.

A.2 Empirical error and success distributions

In this section, we provide the plots, analogous to Figure 1 in the main paper, that show the distribution of the confidence measures over correct and incorrect predictions respectively, for each dataset and each model in our failure prediction experiments. We also include absolute numbers of incorrect and correct predictions grouped into 3 bins (' $> 1/K$ ', ' $[\frac{1}{K}, \frac{1}{2}]$ ' and ' $> 1/2$ ') to validate our theoretical assumptions about TCP's properties. The plots are available

for MNIST with MLP in Fig. 7, for MNIST with a small convnet in Fig. 8, for SVHN with a small convnet in Fig. 9, for CIFAR-100 with VGG-16 in Fig. 10 and for CamVid with SegNet in Fig. 11.

APPENDIX B

EXPERIMENTS ON FAILURE PREDICTION

B.1 Implementation details

Datasets. We run experiments on image datasets of varying scale and complexity: MNIST [58] and SVHN [59] datasets provide relatively simple and small (28×28) images of digits (10 classes). They are split in 60,000 training samples and 10,000 testing samples. CIFAR-10 and CIFAR-100 [60] bring more complexity to classify low resolution images. In each dataset, we further keep 10% of training samples as a validation dataset. We also report experiments for semantic segmentation on CamVid [67], using ConfidNet's training and architecture introduced in Section 4 of the main paper, with dense layers replaced by 1×1 convolutions with adequate number of channels. CamVid is a standard road scene dataset. Images are resized to 360×480 pixels and are segmented according to 11 classes such as 'road', 'building', 'car' or 'pedestrian'.

Classification network. For each dataset, we use standard neural network architectures as classifiers. We reimplemented in PyTorch [66] the network architectures proposed in [24] for fair comparison. They range from small convolutional networks for MNIST¹ and SVHN² to VGG-16 architectures³ for CIFAR datasets. We also added a multi-layer perceptron (MLP) with 1 hidden layer of size 100 for MNIST dataset in order to investigate performances on small models. Finally, we implemented SegNet following [25]. All models are trained in a standard way with a cross-entropy loss and an SGD optimizer with a learning rate of 10^{-3} , a momentum of 0.9 and a weight decay of 10^{-4} . The number of training epochs depends on the dataset considered, varying from 100 epochs on MNIST to 250 epochs on CIFAR-100. As we also want to compute Monte Carlo samples following [19], we include dropout layers. Best models are selected on validation-set accuracy.

ConfidNet. For each of the considered classification models, ConfidNet is built upon the penultimate layer, which is a convolutional layer with non-linear activation and optionally followed by a normalization layer. We train ConfidNet for 100 epochs with Adam optimizer with learning rate 1×10^{-4} , dropout, weight decay 10^{-4} and same data augmentation as in classifier's training. We select the best model based on the AUPR on the validation dataset. In the second training step involving encoder fine-tuning, the training is completed on very few epochs based on previous best model, using Adam optimizer with learning rate 1×10^{-6} or 1×10^{-7} and no dropout to mitigate stochastic effects that may lead the new encoder to deviate too much from the original one used for classification. Once again, the best model is selected on validation-set AUPR.

1. <https://github.com/EN10/KerasMNIST>

2. <https://github.com/tohinz/SVHN-Classifier>

3. <https://github.com/geifmany/cifar-vgg>

Fig. 7: **Distributions of MCP and TCP confidence estimates.** These distributions are computed over correct and erroneous predictions by a trained MLP on MNIST.

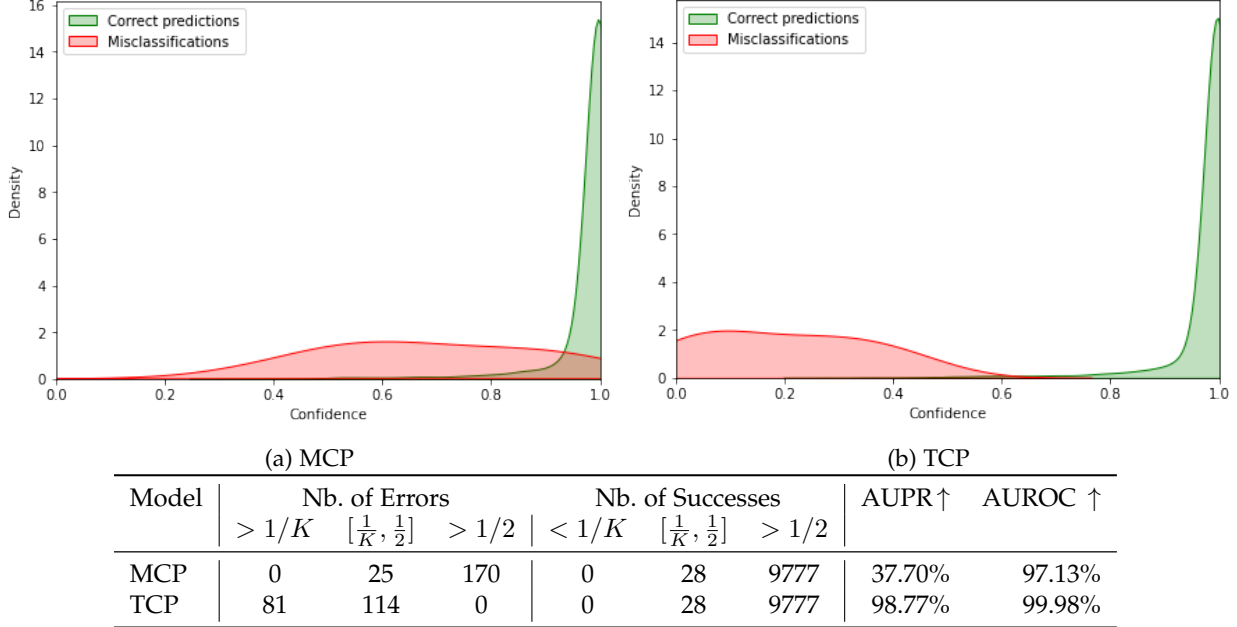
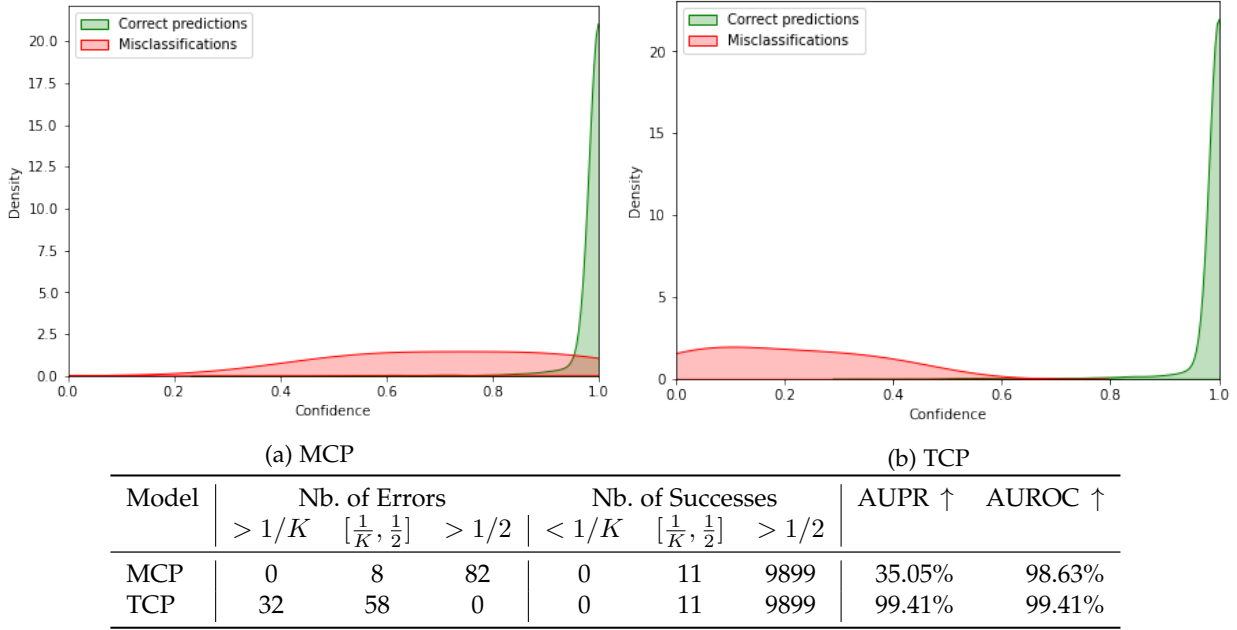


Fig. 8: Same as Figure 7 on MNIST using a small convnet architecture.



Other baseline details. For Trust Score [24], we used the code provided by the authors⁴. We add parallel processing when computing distances for each class to speed up inference. This parallelization does not alter the algorithm nor its performance. Specifically for semantic segmentation with CamVid, each image contains 172,800 pixels. Even though CamVid remains a small dataset (367 training images, 101 validation images, 233 test images) compared to other semantic segmentation datasets, computation complexity forced us to drastically reduce the number of training neighbors and the number of test samples. We randomly sample in each train and test image a small percentage of pixels to compute a proxy.

For MC Dropout [19], we use the same model than baseline (which already includes dropout layers) and we sample 100 times from the classification model at test time keeping dropout layers activated. We then compute the average softmax probability over all samples to conduct Monte Carlo integration. Model uncertainty is estimated, following [19], by calculating the entropy of the averaged probability vector across the class dimension.

4. <https://github.com/google/TrustScore>

Fig. 9: Same as Figure 7 on SVHN using a small convnet architecture.

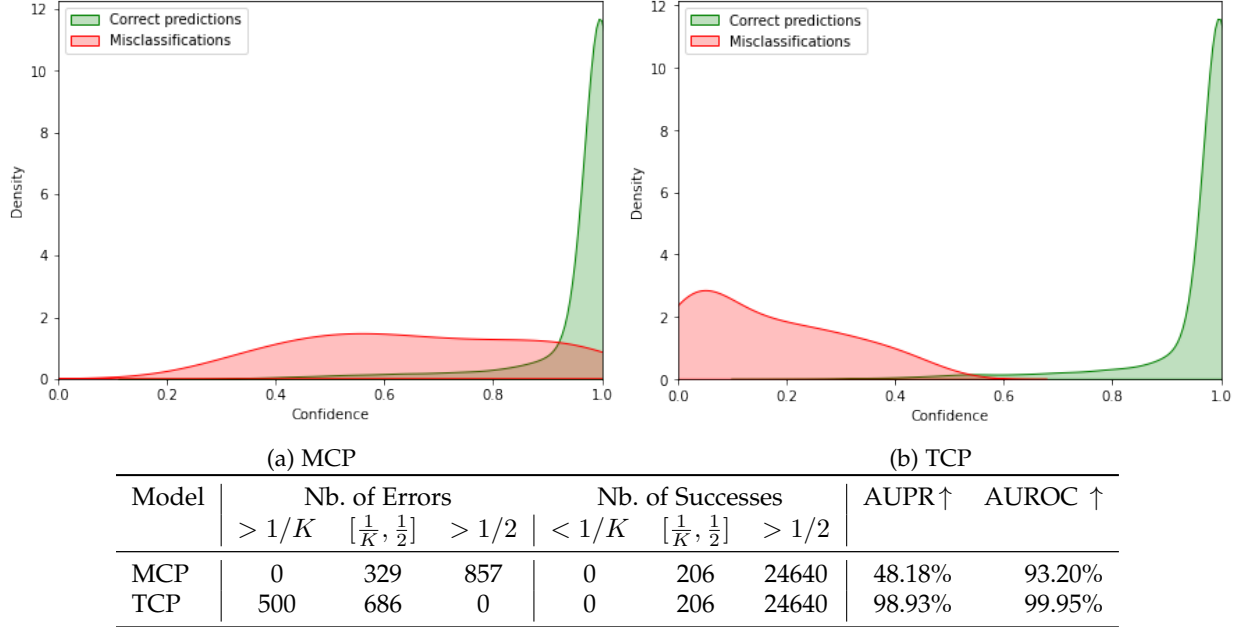
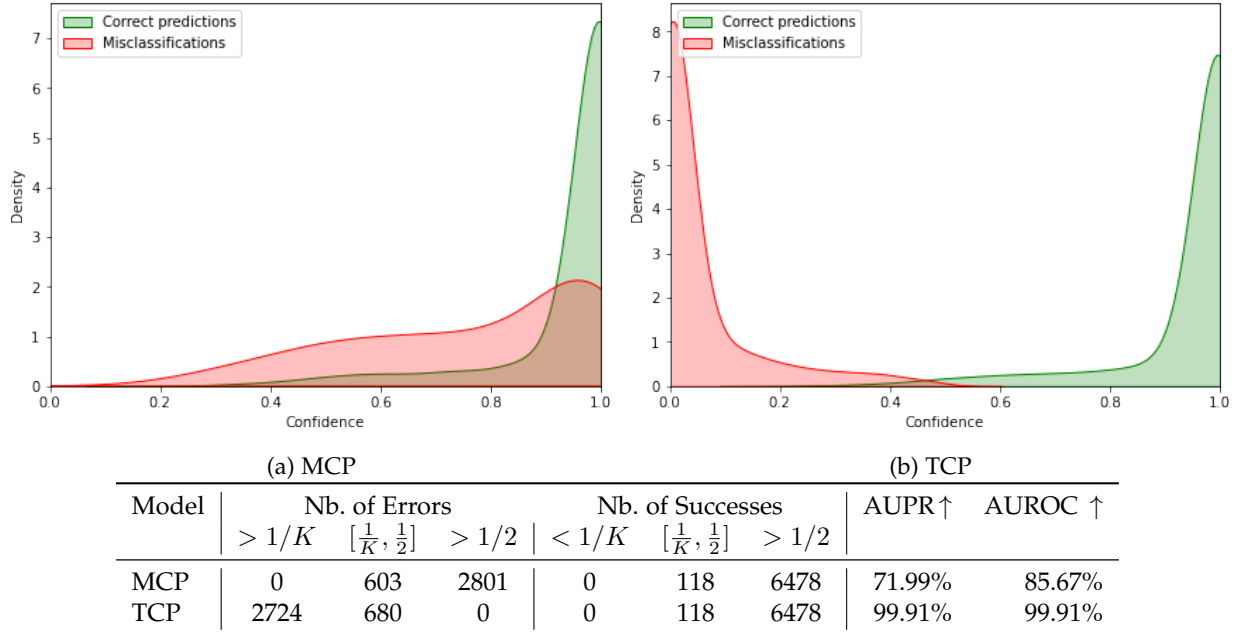


Fig. 10: Same as Figure 7 on CIFAR-100 using a VGG-16 architecture.



B.2 Evaluation metrics

Failure prediction being the task of detecting samples that have been incorrectly classified by the main model (if their estimated confidence is below a chosen threshold δ), classic detection metrics can be used.

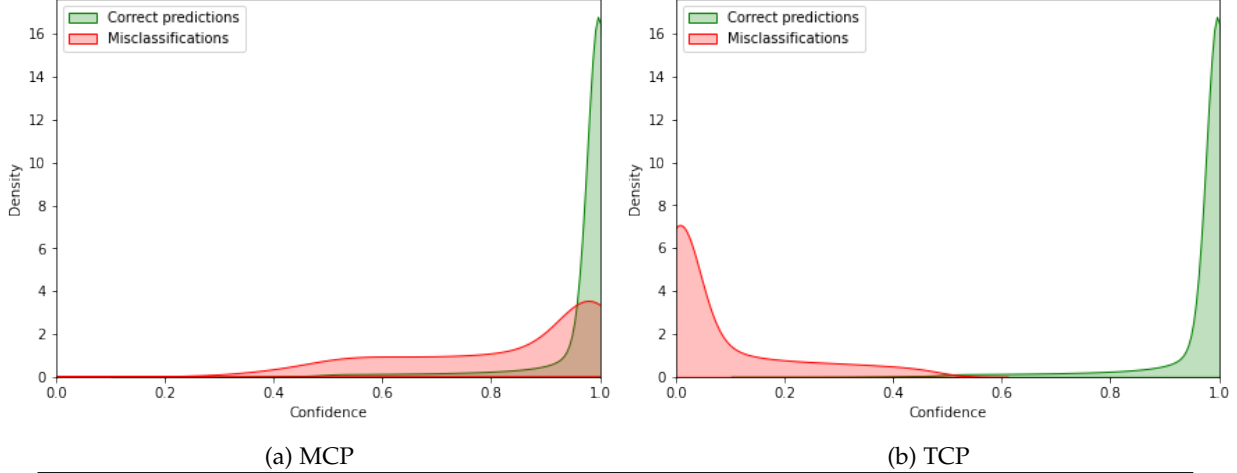
False-positive rate at 95% true-positive rate (FPR@95% TPR). This is the probability that an image predicted incorrectly by the model is wrongly seen as correctly classified by the error detector (a false positive) while the true positive rate is as high as 95%. True- and false-positive rates are defined as $\text{TPR} = \text{TP}/(\text{TP} + \text{FN})$ and $\text{FPR} = \text{FP}/(\text{FP} + \text{TN})$, where TP , TN , FP and FN are

the numbers of true positives, true negatives, false positives and false negatives respectively.

Area under the receiver operating characteristic curve (AUROC). The receiver operating characteristic (ROC) curve is the graph of TPR as function of FPR. This metric is threshold-independent. It can be interpreted as the probability that an incorrectly classified sample has a greater prediction score than a negative example.

Area under the precision-recall curve (AUPR). The precision-recall (PR) curve is the graph of the precision = $\text{TP}/(\text{TP} + \text{FP})$ as a function of the recall = $\text{TP}/(\text{TP} + \text{FN})$. In our experiments, classification errors are used as the

Fig. 11: Same as Figure 7 on CamVid using a SegNet architecture.



Model	Nb. of Errors			Nb. of Successes			AUPR↑	AUROC↑
	> 1/K	[1/K, 1/2]	> 1/2	< 1/K	[1/K, 1/2]	> 1/2		
MCP	0	401,573	55,506,172	0	188,128	34,166,526	48.53%	84.42%
TCP	41,84,875	1,722,871	0	0	188,128	34,166,526	99.92%	99.99%

TABLE 7: **Accuracies for used classification models.** Image classification accuracies on train, validation and test sets for all the models whose confidence is estimated in our experiments.

	MNIST MLP	MNIST SmallConvNet	SVHN SmallConvNet	CIFAR-10 VGG-16	CIFAR-100 VGG-16	CamVid SegNet
Train accuracy	98.32%	98.94%	95.06%	98.69%	95.55%	96.69%
Validation accuracy	97.95%	99.03%	96.56%	99.80%	66.96%	91.72%
Test accuracy	98.05%	99.10%	95.44%	92.19%	65.96%	85.33%

TABLE 8: **Impact of the encoder fine-tuning on the error-prediction performance of ConfidNet.** Comparison in AUPR (the higher, the better) on all benchmarks. This table extends Table 3 in the main paper.

	MNIST MLP	MNIST SmallConvNet	SVHN SmallConvNet	CIFAR-10 VGG-16	CIFAR-100 VGG-16	CamVid SegNet
Confidence training	57.34%	43.94%	50.43%	46.44%	72.68%	50.12%
+ Fine-tuning ConvNet	57.37%	45.89%	50.72%	49.94%	73.68%	50.51%

positive detection class. As we specifically want to detect failures, AUPR is the primary metrics to assess performances.

Area under the risk-coverage curve (AURC). In classification with a reject option, the risk-coverage curve is the graph of the empirical risk of the classifier given a loss (usually 0/1 loss) as a function of the empirical coverage, which is the proportion of the non-rejected samples. This metric is threshold-independent, as AUROC and AUPR.

Excess-AURC (E-AURC). This is a normalized AURC metrics defined in [61]. It takes into account the optimal ranking given the error rate of the classifier. More specifically, if we denote κ_f^* the perfect confidence-rate function and \hat{r} the risk of classifier f , it writes as:

$$E\text{-AURC}(\kappa_f) = \text{AURC}(\kappa_f) - \text{AURC}(\kappa_f^*) \quad (20)$$

$$\approx \text{AURC}(\kappa_f) - (\hat{r} + (1 - \hat{r}) \log(1 - \hat{r})). \quad (21)$$

B.3 Classification accuracies of model F

Most neural networks used in our experiments tend to overfit. On small datasets such as MNIST and SVHN, convolutional neural networks already achieve nearly perfect accuracy on test set, above 96%, which leaves very few errors available. We provide in Table 7 the accuracies on training, validation and test set of the classification model F whose confidence must be predicted.

B.4 Effect of ConfidNet's architecture

We experiment different architectures for ConfidNet on the SVHN dataset, varying the number of layers. Except for the first and last layers, whose dimensions respectively depend on the size of the input and of the output, each layer presents the same number of units (400). On Figure 12, we observe that starting from 3 layers, ConfidNet already improves baseline performance.

TABLE 9: **Effect of the loss and of the confidence criterion on the error-detection performance of ConfidNet.** Comparison in between proposed MSE and three other alternatives, all based on TCP as confidence criterion. Using MSE with normalized TCP^r is also reported. This table extends Table 5 in the main paper.

Dataset	Loss	FPR @ 95% TPR ↓	AUPR ↑	AUROC ↑
SVHN SmallConvNet	MSE	28.58%	50.72%	93.44%
	BCE	29.34%	50.00%	92.76%
	Focal	28.67%	49.96%	93.01%
	Ranking	31.04%	48.11%	92.90%
	MSE w/ TCP ^r	30.19%	47.04%	93.12%
CIFAR-10 VGG-16	MSE	44.94%	49.94%	92.12%
	BCE	45.20%	47.95%	91.94%
	Focal	45.20%	47.76%	91.93%
	Ranking	46.99%	44.04%	91.49%
	MSE w/ TCP ^r	44.43%	48.78%	92.19%
CamVid SegNet	MSE	61.52%	50.51%	85.02%
	BCE	61.68%	48.96%	83.41%
	Focal	61.64%	49.05%	84.09%
	MSE w/ TCP ^r	60.41%	51.35%	85.18%

TABLE 10: **Comparative calibration results.** Performance in ECE (the lower, the better) when using MCP baseline ('Baseline') or ConfidNet as confidence estimator on the six benchmarks, and when using dedicated temperature scaling ('T. Scaling').

	MNIST MLP	MNIST SmallConvNet	SVHN SmallConvNet	CIFAR-10 VGG-16	CIFAR-100 VGG-16	CamVid SegNet
Baseline	0.37%	0.20%	0.50%	4.48%	22.37%	9.65%
ConfidNet	0.66%	0.30%	1.11%	3.45%	15.61%	7.57%
Baseline + T. Scaling	0.20%	0.69%	1.30%	2.88%	5.16%	4.77%

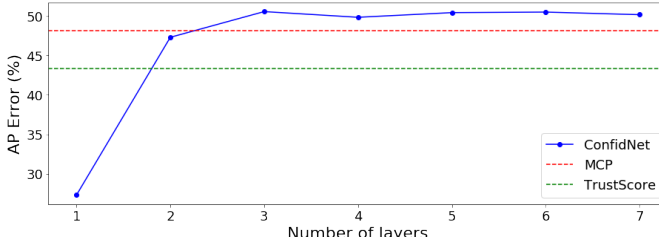


Fig. 12: **Influence of ConfidNet's depth on its performance.** Performance in AUPR as a function of the number of layers used in ConfidNet on SVHN test set and compared to the performance of MCP and True Score baselines.

B.5 Effect of learning variants

In Table 8, we detail the effect of fine-tuning on all classification and segmentation datasets for failure prediction experiments.

The influence of the loss (MSE, BCE, Focal Loss or Ranking based on TCP) is analysed for SVHN, CIFAR10 and CamVid in Table 9. We also tested a normalized variant of the TCP confidence criterion, which consists in the *ratio* between TCP and MCP:

$$\text{TCP}_F^r(\mathbf{x}, y) = \frac{F(\mathbf{x}; \hat{\mathbf{w}})[y]}{\max_{k \in \mathcal{Y}} F(\mathbf{x}; \hat{\mathbf{w}})[k]}. \quad (22)$$

This criterion presents stronger theoretical guarantees than TCP, since correct predictions will be, by design, assigned a confidence of 1, whereas errors' confidence will lie in $[0, 1]$. On the other hand, learning this criterion may be more challenging since all correct predictions have a unique target confidence value. We note in Table 8 that its performance

is lower than the one of TCP on small datasets such as CIFAR-10 where few errors are present, but higher on larger datasets such as CamVid where each pixel is a sample. This emphasizes once again the complexity of incorrect/correct classification training.

B.6 Effect on calibration

We observed that ConfidNet tends to lower the confidence of an example that the model wrongly classified while being over-confident (high MCP). As a side experiment, we study whether using ConfidNet as confidence estimation can improve the calibration of deep neural networks.

In Table 10, we report the expected calibration error (ECE) which is an approximate measure of miscalibration between confidence and accuracy [35]. ConfidNet yields equivalent or better ECE results than the MCP baseline, with clear superiority on complex datasets such as CIFAR-10, CIFAR-100 and CamVid. On MNIST and SVHN, the baseline already offers a small ECE. These results confirm our intuition about the capacity of ConfidNet to address over-confident predictions, even though it has not been designed for. Nevertheless, dedicated methods such as temperature scaling used in [35] remain preferred for calibrating deep neural networks.

B.7 Qualitative assessment

We provide in Figure 13 an illustration of confidence-based failure prediction on CamVid. Compared to the MCP baseline, our approach produces higher confidence scores for pixels correctly classified by DeepLabv2 and lower ones for incorrectly classified ones. This allows one to better identify

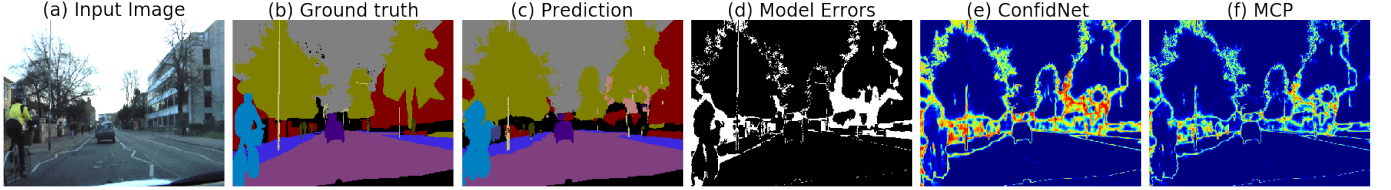


Fig. 13: **Confidence estimation in semantic segmentation.** On this example from CamVid (a), the confidence at each pixel of the class prediction delivered by DeepLabv2 (c) can be done classically by MCP (f), or by the proposed auxiliary model (e). The second approach appears better aligned with the actual errors (shown in white in (d)) of the semantic segmentation. Indeed, ConfidNet (50.51% AUPR) allows a better prediction of these errors than MCP (48.53%).

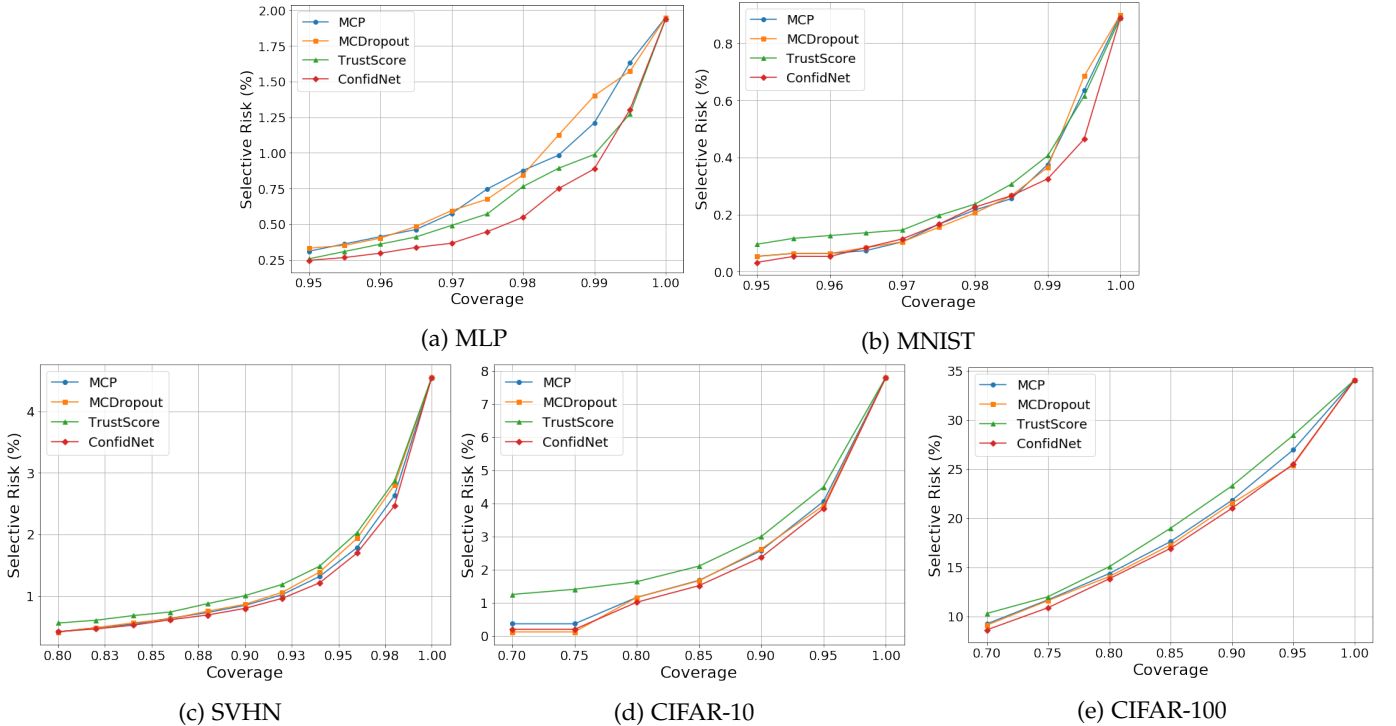


Fig. 14: **Risk-coverage curves of selective image classification.** On the five benchmarks, the RC curves are provided for MCP baseline, MC Dropout, Trust Score and ConfidNet. For a given coverage (fraction of non-rejected samples), the selective risk indicates the percentage of erroneous predictions in the remaining test set.

error areas in semantic segmentation maps, as we leverage in ConDA.

B.8 Risk-coverage curves

In relation with the selective classification experiments, we provide the risk-coverage curves for five classification benchmarks: MLP on MNIST (Fig. 14a), SmallConvNet on MNIST (Fig. 14b), SmallConvNet on SVHN (Fig. 14c) and VGG-16 on CIFAR-10 and CIFAR-100 (Figs. 14d and 14e).

APPENDIX C EXPERIMENTS WITH SELF-TRAINING FOR UNSUPERVISED DOMAIN ADAPTATION

C.1 Experiments details

The segmentation network is a DeepLabv2 [57] architecture, optimized by stochastic gradient descent with learning rate 2.5×10^{-4} , momentum 0.9 and weight decay 10^{-4} .

As in recent state-of-the-art methods [21], [49], [50], we adopt an adversarial learning approach to align source and target output distributions. The discriminator in the segmentation network is optimized by Adam [68] with learning rate 10^{-4} . The hyperparameters λ_{adv} and λ_{ST} are fixed at 10^{-3} and 1, respectively. In Table 5 of the main paper, CBST results [53] are drawn from the authors' most recent paper [54] where CBST serves as baseline.

Self-training procedure. Following the implementation in BDL [21], we carried out 2 self-training iterations for AdvEnt in GTA5 \triangleright Cityscapes experiments. For the other experiments in Section C.3 below, only 1 self-training iteration is used.

The experiments start by pre-training AdvEnt model, using the published code, on source-domain images translated into the target domain. Those translated images are pre-computed using a CycleGAN [69], as provided by [21].⁵

5. <https://github.com/liyunsheng13/BDL>

TABLE 11: **Ablation study on semantic segmentation with pseudo-labeling-based adaptation.** This table extends Tab. 6 in the main paper by providing IoUs for the 19 classes of the GTA5 \triangleright Cityscapes UDA benchmark, using AdapSegNet model.

Method	Multi-Scale	Adv Training	GTA5 \triangleright Cityscapes																			mIoU
			road	sidewalk	building	wall	fence	pole	light	sign	veg	terrain	sky	person	rider	car	truck	bus	train	mbike	bike	
ConfidNet	✓		88.9	44.4	84.6	34.3	26.2	32.8	39.0	32.5	84.9	33.6	82.8	59.8	31.7	80.9	30.3	45.9	0.0	30.9	40.8	47.6
Multi-Scale ConfidNet	✓		91.1	48.1	85.2	34.7	25.3	34.8	41.1	35.0	85.5	41.3	82.9	59.5	32.8	83.7	27.6	44.0	0.0	28.6	41.3	48.5
Adv. ConfidNet	✓	✓	90.8	49.6	84.5	34.6	28.6	32.7	40.0	31.3	84.4	37.6	83.9	59.7	33.3	82.9	35.2	47.6	1.2	30.2	44.3	49.1
ConDA (Adv. Multi-Scale)	✓	✓	90.8	48.2	85.5	40.0	31.2	33.3	40.3	33.9	84.8	39.4	85.3	59.1	32.2	83.3	28.2	44.6	0.1	32.0	47.0	49.4

TABLE 12: **Additional comparative performance on semantic segmentation with synth-to-real unsupervised domain adaptation.** Results in per-class IoU and aggregated mIoU on SYNTHIA \triangleright Cityscapes ('mIoU*' is the 13-class setup, excluding the classes 'wall', 'fence' and 'pole', as used in earlier works). All methods are based on a DeepLabv2 backbone.

Method	Self-Train.	SYNTHIA \triangleright Cityscapes																			mIoU	mIoU*
		road	sidewalk	building	wall	fence	pole	light	sign	veg	sky	person	rider	car	bus	mbike	bike					
AdaptSegNet [49]		84.3	42.7	77.5	-	-	-	4.7	7.0	77.9	82.5	54.3	21.0	72.3	32.2	18.9	32.3	-	-	46.7		
DISE [62]		91.7	53.5	77.1	2.5	0.2	27.1	6.2	7.6	78.4	81.2	55.8	19.2	82.3	30.3	17.1	34.3	41.5	48.8			
AdvEnt [50]		85.6	42.2	79.7	8.7	0.4	25.9	5.4	8.1	80.4	84.1	57.9	23.8	73.3	36.4	14.2	33.0	41.2	48.0			
CBST [53]	✓	68.0	29.9	76.3	10.8	1.4	33.9	22.8	29.5	77.6	78.3	60.6	28.3	81.6	23.5	18.8	39.8	42.6	48.9			
MRKLD [54]	✓	67.7	32.2	73.9	10.7	1.6	37.4	22.2	31.2	80.8	80.5	60.8	29.1	82.8	25.0	19.4	45.3	43.8	50.1			
BDL [21]	✓	83.9	43.7	80.2	12.9	0.5	30.1	18.0	17.3	79.7	83.5	52.2	25.8	72.5	35.5	25.8	45.4	44.2	51.0			
ConDA	✓	88.1	46.7	81.1	10.6	1.1	31.3	22.6	19.6	81.3	84.3	53.9	21.7	79.8	42.9	24.2	46.8	46.0	53.3			

C.2 Detailed ablation study

We complement the ablation results in Table 6 of the main paper, by providing class-wise IoUs in Table 11.

C.3 Additional results

We extend our experiments by using another synthetic source-domain dataset, SYNTHIA [70]. More specifically, we use the SYNTHIA-RAND-CITYSCAPES split, composed of 9,400 color images generated in a simulator, of dimension 1280×760 and annotated for semantic segmentation with 16 classes in common with Cityscapes [64]. In the experiments with this dataset, we do not use translated source images.

SYNTHIA \triangleright Cityscapes. Similar to Table 4 in the main paper, we report in Table 12 the comparative results on SYNTHIA \triangleright Cityscapes. Following the literature on this dataset, mIoU metric is computed over 16 categories as well as over 13 categories (ignoring 'wall', 'fence' and 'pole'). Again, ConDA achieves impressive performance for methods with a DeepLabv2 backbone on this benchmark with 46.0% mIoU.

SYNTHIA \triangleright Mapillary. Along with previous results on Cityscapes, we further study domain adaptation on another target dataset. Mapillary Vistas [65] is a dataset of street-level images, split in a train set, a validation set and a test set. The ground-truth semantic maps are missing from the test set. For domain adaptation, we use the 18,000 images from the training set as target and the 2,000 images from the validation set for testing. We consider 7 'super classes' that include the 16 classes used in Cityscapes [64] experiments with SYNTHIA [70]. Table 13 presents semantic segmentation results using SYNTHIA as source dataset. This benchmark has also been used in other recent works, such as in AdvEnt [50] and DADA [71]. ConDA outperforms

TABLE 13: **Combining ConDA with AdvEnt and DADA approaches to domain adaptation in semantic segmentation.** Performance in IoU and mIoU on SYNTHIA \triangleright Mapillary. 'DADA*' and 'ConDA*' are trained using depth as privileged information.

Method	Self-Train.	SYNTHIA \triangleright Mapillary							mIoU
		flat	constr.	object	nature	sky	human	vehicle	
AdvEnt [50]		86.9	58.8	30.5	74.1	85.1	48.3	72.5	65.2
ConDA	✓	89.1	63.5	28.3	72.7	88.2	49.7	73.0	66.4
DADA* [71]		86.7	62.1	34.9	75.9	88.6	51.1	73.8	67.6
ConDA*	✓	87.8	67.5	40.5	76.8	92.3	60.7	78.5	72.0

baseline methods with 66.4% mIoU compared to 65.2% mIoU in AdvEnt.

We also tested the proposed confidence-based self-training approach on DADA [71], another domain adaptation baseline which uses the depth information available on source-domain synthetic scenes as privileged information during segmentation training. Again, the proposed method (ConDA*) provides a boost of performance, from 67.6% to 72.0% mIoU.

C.4 Additional model analysis

In this section, we provide additional plots analogous to those in Figure 7 of the main paper. These graphs show precision w.r.t. coverage of extracted pseudo-labels, using MCP and ConDA respectively, in the following set-ups:

- AdvEnt on SYNTHIA \triangleright Cityscapes (Figure 15);
- AdvEnt on SYNTHIA \triangleright Mapillary Vistas (Figure 16);
- DADA on SYNTHIA \triangleright Mapillary Vistas (Figure 17).

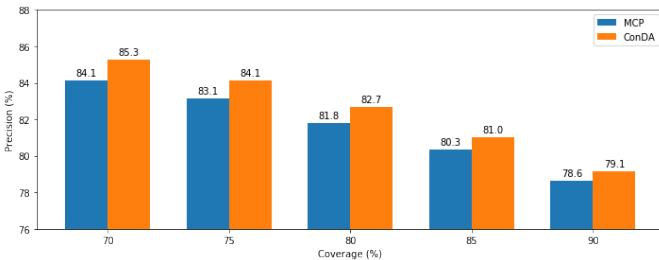


Fig. 15: **Comparative quality of selected pseudo-labels.** Proportion of correct pseudo-labels (precision) for different coverages on SYNTHIA > Cityscapes for AdvEnt.

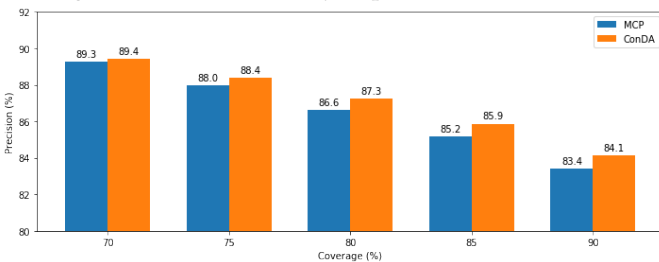


Fig. 16: Same as Fig. 15 for AdvEnt on SYNTHIA > Mapillary

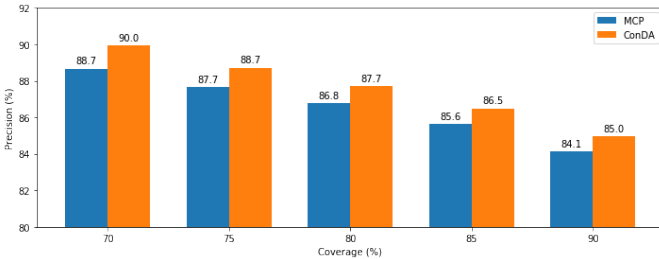


Fig. 17: Same as Fig. 15 for DADA on SYNTHIA > Mapillary

In all cases, we observe that ConDA collects fewer erroneous pseudo-labels than MCP.

REFERENCES

- [1] A. Krizhevsky, I. Sutskever, and G. Hinton, "ImageNet classification with deep convolutional neural networks," in *NIPS*, 2012. 1, 10
- [2] S. Ren, K. He, R. Girshick, and J. Sun, "Faster r-cnn: Towards real-time object detection with region proposal networks," in *NIPS*, 2015. 1
- [3] W. Liu, D. Anguelov, D. Erhan, C. Szegedy, S. Reed, C.-Y. Fu, and A. C. Berg, "Ssd: Single shot multibox detector," in *ECCV*, 2016. 1
- [4] J. Redmon, S. K. Divvala, R. B. Girshick, and A. Farhadi, "You only look once: Unified, real-time object detection," in *CVPR*, 2016. 1
- [5] T. Mikolov, K. Chen, G. Corrado, and J. Dean, "Efficient estimation of word representations in vector space," *CoRR*, 2013. 1
- [6] T. Mikolov, M. Karafiat, L. Burget, J. Cernocky, and S. Khudanpur, "Recurrent neural network based language model," in *INTERSPEECH*, 2010. 1
- [7] G. Hinton, L. Deng, D. Yu, G. E. Dahl, A.-r. Mohamed, N. Jaitly, A. Senior, V. Vanhoucke, P. Nguyen, T. N. Sainath *et al.*, "Deep neural networks for acoustic modeling in speech recognition: The shared views of four research groups," *IEEE Signal Process Mag*, 2012. 1
- [8] A. Hannun, C. Case, J. Casper, B. Catanzaro, G. Diamos, E. Elsen, R. Prenger, S. Satheesh, S. Sengupta, A. Coates, and A. Y. Ng, "Deep speech: Scaling up end-to-end speech recognition," 2014. 1
- [9] D. Amodei, C. Olah, J. Steinhardt, P. F. Christiano, J. Schulman, and D. Mané, "Concrete problems in AI safety," *CoRR*, 2016. 1
- [10] J. Janai, F. Güney, A. Behl, and A. Geiger, "Computer vision for autonomous vehicles: Problems, datasets and state-of-the-art," *Foundations and Trends in Computer Graphics and Vision*, 2017. 1
- [11] J. Nam, S. Park, E. J. Hwang, J. Lee, K.-N. Jin, K. Lim, T. Vu, J. Sohn, S. Hwang, J. M. Goo, and C. M. Park, "Development and validation of deep learning-based automatic detection algorithm for malignant pulmonary nodules on chest radiographs," *Radiology*, 2018. 1
- [12] O. Linda, T. Vollmer, and M. Manic, "Neural network based intrusion detection system for critical infrastructures," in *IJCNN*, 2009. 1
- [13] C. Chow, "An optimum character recognition system using decision functions," *IRE Trans. Electron. Comput.*, 1957. 1, 2
- [14] P. L. Bartlett and M. H. Wegkamp, "Classification with a reject option using a hinge loss," *JMLR*, 2008. 1, 2
- [15] C. Cortes, G. DeSalvo, and M. Mohri, "Boosting with abstention," in *NIPS*, 2016. 1, 2
- [16] R. El-Yaniv and Y. Wiener, "On the foundations of noise-free selective classification," *JMLR*, 2010. 1, 2, 4
- [17] Y. Geifman and R. El-Yaniv, "Selective classification for deep neural networks," in *NIPS*, 2017. 1, 2, 4
- [18] Y. Gal, R. Islam, and Z. Ghahramani, "Deep Bayesian active learning with image data," in *Proceedings of Machine Learning Research*, 2017. 1
- [19] Y. Gal and Z. Ghahramani, "Dropout as a bayesian approximation: Representing model uncertainty in deep learning," in *ICML*, 2016. 1, 2, 8, 9, 12, 13
- [20] D.-H. Lee, "Pseudo-label : The simple and efficient semi-supervised learning method for deep neural networks," *ICML (Workshop)*, 2013. 1, 3
- [21] Y. Li, L. Yuan, and N. Vasconcelos, "Bidirectional learning for domain adaptation of semantic segmentation," in *CVPR*, 2019. 1, 3, 10, 17, 18
- [22] S. Hecker, D. Dai, and L. V. Gool, "Failure prediction for autonomous driving," in *IV*, 2018. 1
- [23] D. Hendrycks and K. Gimpel, "A baseline for detecting misclassified and out-of-distribution examples in neural networks," *ICLR*, 2017. 1, 2, 8, 9
- [24] H. Jiang, B. Kim, M. Guan, and M. Gupta, "To trust or not to trust a classifier," in *NIPS*, 2018. 1, 2, 8, 9, 12, 13
- [25] A. Kendall, V. Badrinarayanan, , and R. Cipolla, "Bayesian segnet: Model uncertainty in deep convolutional encoder-decoder architectures for scene understanding," *arXiv preprint arXiv:1511.02680*, 2015. 1, 12
- [26] A. Ragni, Q. Li, M. J. F. Gales, and Y. Wang, "Confidence estimation and deletion prediction using bidirectional recurrent neural networks," in *SLT Workshop*, 2018. 1
- [27] Q. Li, P. Ness, A. Ragni, and M. Gales, "Bi-directional lattice recurrent neural networks for confidence estimation," in *ICASSP*, 2018. 1
- [28] D. Yu, J. Li, and L. Deng, "Calibration of confidence measures in speech recognition," *IEEE Trans Audio Speech Lang Process*, 2011. 1
- [29] J. Blatz, E. Fitzgerald, G. Foster, S. Gandrabur, C. Goutte, A. Kulesza, A. Sanchis, and N. Ueffing, "Confidence estimation for machine translation," in *COLING*, 2004. 1, 2
- [30] C. Corbière, N. Thome, A. Bar-Hen, M. Cord, and P. Pérez, "Addressing failure prediction by learning model confidence," in *NeurIPS*, 2019. 2
- [31] C. Cortes, G. DeSalvo, and M. Mohri, "Learning with rejection," in *ALT*, 2016. 2
- [32] H. Zaragoza and d. Buc, "Confidence measures for neural network classifiers," in *IPMU*, 1998. 2
- [33] Y. Geifman and R. El-Yaniv, "Selectivenet: A deep neural network with an integrated reject option," in *ICML*, 2019. 2
- [34] A. M. Nguyen, J. Yosinski, and J. Clune, "Deep neural networks are easily fooled: High confidence predictions for unrecognizable images," in *CVPR*, 2015. 2
- [35] C. Guo, G. Pleiss, Y. Sun, and K. Q. Weinberger, "On calibration of modern neural networks," in *ICML*, 2017. 2, 5, 16
- [36] L. Neumann, A. Zisserman, and A. Vedaldi, "Relaxed softmax: Efficient confidence auto-calibration for safe pedestrian detection," in *NIPS (Workshop)*, 2018. 2
- [37] I. Goodfellow, J. Shlens, and C. Szegedy, "Explaining and harnessing adversarial examples," in *ICLR*, 2015. 2
- [38] C. Szegedy, W. Zaremba, I. Sutskever, J. Bruna, D. Erhan, I. J. Goodfellow, and R. Fergus, "Intriguing properties of neural networks," in *ICLR*, 2014. 2

[39] S. Liang, Y. Li, and R. Srikant, "Enhancing the reliability of out-of-distribution image detection in neural networks," in *ICLR*, 2018. 2

[40] B. Lakshminarayanan, A. Pritzel, and C. Blundell, "Simple and scalable predictive uncertainty estimation using deep ensembles," in *NIPS*, 2017. 2

[41] R. M. Neal, *Bayesian Learning for Neural Networks*. Springer, 1996. 2

[42] C. Blundell, J. Cornebise, K. Kavukcuoglu, and D. Wierstra, "Weight uncertainty in neural networks," in *ICML*, 2015. 2

[43] W. J. Maddox, P. Izmailov, T. Garipov, D. P. Vetrov, and A. G. Wilson, "A simple baseline for Bayesian uncertainty in deep learning," in *NeurIPS*, 2019. 2

[44] J. M. Hernandez-Lobato and R. Adams, "Probabilistic backpropagation for scalable learning of Bayesian neural networks," in *ICML*, 2015. 2

[45] L. P. Cordella, C. De Stefano, F. Tortorella, and M. Vento, "A method for improving classification reliability of multilayer perceptrons," *IEEE Transactions on Neural Networks*, 1995. 2

[46] K. Beyer, J. Goldstein, R. Ramakrishnan, and U. Shaft, "When is 'nearest neighbor' meaningful?" in *ICDT*, 1999. 2

[47] T. DeVries and G. W. Taylor, "Learning confidence for out-of-distribution detection in neural networks," *arXiv preprint arXiv:1802.04865*, 2018. 2

[48] J. Hoffman, E. Tzeng, T. Park, J.-Y. Zhu, P. Isola, K. Saenko, A. A. Efros, and T. Darrell, "Cycada: Cycle consistent adversarial domain adaptation," in *ICML*, 2018. 3, 10

[49] Y.-H. Tsai, W.-C. Hung, S. Schulter, K. Sohn, M.-H. Yang, and M. Chandraker, "Learning to adapt structured output space for semantic segmentation," in *CVPR*, 2018. 3, 10, 17, 18

[50] T.-H. Vu, H. Jain, M. Bucher, M. Cord, and P. Pérez, "Advent: Adversarial entropy minimization for domain adaptation in semantic segmentation," in *CVPR*, 2019. 3, 10, 17, 18

[51] Y. Grandvalet and Y. Bengio, "Semi-supervised learning by entropy minimization," in *NIPS*, 2005. 3

[52] A. Saporta, T.-H. Vu, M. Cord, and P. Pérez, "Esl: Entropy-guided self-supervised learning for domain adaptation in semantic segmentation," 2020. 3, 10

[53] Y. Zou, Z. Yu, B. Vijaya Kumar, and J. Wang, "Unsupervised domain adaptation for semantic segmentation via class-balanced self-training," in *ECCV*, 2018. 3, 10, 17, 18

[54] Y. Zou, Z. Yu, X. Liu, B. V. Kumar, and J. Wang, "Confidence regularized self-training," in *ICCV*, 2019. 3, 10, 17, 18

[55] P. Mohapatra, M. Rolínek, C. Jawahar, V. Kolmogorov, and M. Pawan Kumar, "Efficient optimization for rank-based loss functions," in *CVPR*, 2018. 5

[56] T. Lin, P. Goyal, R. Girshick, K. He, and P. Dollár, "Focal loss for dense object detection," in *ICCV*, 2017. 5

[57] L.-C. Chen, G. Papandreou, I. Kokkinos, K. Murphy, and A. L. Yuille, "Deeplab: Semantic image segmentation with deep convolutional nets, atrous convolution, and fully connected crfs," *CoRR*, 2016. 8, 17

[58] Y. Lecun, L. Bottou, Y. Bengio, and P. Haffner, "Gradient-based learning applied to document recognition," in *Proceedings of the IEEE*, 1998. 8, 12

[59] Y. Netzer, T. Wang, A. Coates, A. Bissacco, B. Wu, and A. Y. Ng, "Reading digits in natural images with unsupervised feature learning," in *NIPS (Workshop)*, 2011. 8, 12

[60] A. Krizhevsky and G. Hinton, "Learning multiple layers of features from tiny images," *Master's thesis, Department of Computer Science, University of Toronto*, 2009. 8, 12

[61] Y. Geifman, G. Uziel, and R. El-Yaniv, "Bias-reduced uncertainty estimation for deep neural classifiers," in *ICLR*, 2019. 9, 15

[62] W.-L. Chang, H.-P. Wang, W.-H. Peng, and W.-C. Chiu, "All about structure: Adapting structural information across domains for boosting semantic segmentation," in *CVPR*, 2019. 10, 18

[63] S. R. Richter, V. Vineet, S. Roth, and V. Koltun, "Playing for data: Ground truth from computer games," in *ECCV*, 2016. 10

[64] M. Cordts, M. Omran, S. Ramos, T. Rehfeld, M. Enzweiler, R. Benenson, U. Franke, S. Roth, and B. Schiele, "The cityscapes dataset for semantic urban scene understanding," in *CVPR*, 2016. 10, 18

[65] G. Neuhold, T. Ollmann, S. Rota Bulò, and P. Kotschieder, "The mapillary vistas dataset for semantic understanding of street scenes," in *ICCV*, 2017. 10, 18

[66] A. Paszke, S. Gross, S. Chintala, G. Chanan, E. Yang, Z. DeVito, Z. Lin, A. Desmaison, L. Antiga, and A. Lerer, "Automatic differentiation in pytorch," in *NIPS (Workshop)*, 2017. 10, 12

[67] G. J. Brostow, J. Fauqueur, and R. Cipolla, "Semantic object classes in video: A high-definition ground truth database," *Pattern Recogn. Lett.*, 2009. 12

[68] J. B. Diederik P. Kingma, "Adam: A method for stochastic optimization," in *ICLR*, 2015. 17

[69] J.-Y. Zhu, T. Park, P. Isola, and A. A. Efros, "Unpaired image-to-image translation using cycle-consistent adversarial networks," in *ICCV*, 2017. 17

[70] G. Ros, L. Sellart, J. Materzynska, D. Vazquez, and A. M. Lopez, "The SYNTHIA dataset: A large collection of synthetic images for semantic segmentation of urban scenes," in *CVPR*, 2016. 18

[71] T.-H. Vu, H. Jain, M. Bucher, M. Cord, and P. Perez, "Dada: Depth-aware domain adaptation in semantic segmentation," in *ICCV*, 2019. 18



Charles Corbière is a Ph.D. student in Deep Learning and Computer Vision for Autonomous Driving at Conservatoire National des Arts et Métiers (CNAM, France) and valeo.ai research lab (France). He received an M.Sc. degree in Applied Mathematics and Statistic by Université Paris-Saclay (France) in 2017 and an M.Eng. degree in Computer Science from Ecole Centrale de Lille (France) in 2016. His research interests include uncertainty in deep learning and certified robustness.



Nicolas Thome is a full professor at Conservatoire National des Arts et Métiers (Cnam Paris). His research interests include machine learning and deep learning for understanding low-level signals, e.g. vision, time series, acoustics, etc. He also explores solutions for combining low-level and more higher-level data for multi-modal data processing. His current application domains are essentially targeted towards healthcare, autonomous driving and physics. He is involved in several French, European and international collaborative research projects on artificial intelligence and deep learning.



Antoine Saporta is a Ph.D. student in Deep Learning and Computer Vision for Autonomous Driving at the Machine Learning and Deep Learning for Information Access (MLIA) team of LIP6, Sorbonne Université (France) and Valeo.ai research lab. He is a graduate of École Polytechnique (France) and has received a Master degree in Computer Science from Technische Universität München (Germany) in 2019. His research interests include domain adaptation and semantic segmentation.



Tuan-Hung Vu is a research scientist at Valeo.ai. He received a PhD degree in Computer Science from École Normale Supérieure in 2018. His research interests include deep learning, object recognition, domain adaptation and more recently data augmentation. Tuan-Hung published and regularly served as reviewer at computer vision conferences and journals like CVPR, ICCV, ECCV and IJCV.



Matthieu Cord is full professor at Sorbonne University. He is also part-time principal scientist at Valeo.ai. His research expertise includes computer vision, machine learning and artificial intelligence. He is the author of more 150 publications on image classification, segmentation, deep learning, and multimodal vision and language understanding. He is an honorary member of the Institut Universitaire de France and served from 2015 to 2018 as an AI expert at CNRS and ANR (National Research Agency).



Patrick Pérez is Scientific Director of Valeo.ai, a Valeo research lab on artificial intelligence for automotive applications. Before joining Valeo, Patrick Pérez has been Distinguished Scientist at Technicolor (2009-2018), researcher at Inria (1993-2000, 2004-2009) and at Microsoft Research Cambridge (2000-2004). His research revolves around machine learning for scene understanding, data mining and visual editing.